Multimodality Imaging of Dementia: Clinical Importance and Role of Integrated Anatomic and Molecular Imaging

Kunal P. Patel, MD
David T. Wymer, MD
Vinay K. Bhatia, MD
Ranjan Duara, MD
Chetan D. Rajadhyaksha, MD

Abbreviations: DLB = dementia with Lewy bodies, FDG = fluorodeoxyglucose, 4R = four repeat, FTLD = frontotemporal lobar degeneration, SNMMI = Society of Nuclear Medicine and Molecular Imaging, 3R = three repeat

RadioGraphics 2020; 40:200–222

https://doi.org/10.1148/rg.2020190070

Content Codes: MR NM NR

From the Department of Radiology, Mount Sinai Medical Center, 4300 Alton Rd, Miami Beach, FL 33140. Presented as an education exhibit at the 2018 RSNA Annual Meeting. Received March 17, 2019; revision requested July 29 and received August 24; accepted August 27. For this journal-based SA-CME activity, the authors, editor, and reviewers have disclosed no relevant relationships. **Address correspondence to** K.P.P. (e-mail: *kunalpatelmd@outlook.com*).

R.D. supported by the National Institute on Aging (5 P50 AG0477266021).

SA-CME LEARNING OBJECTIVES

After completing this journal-based SA-CME activity, participants will be able to:

- List the recommended MRI sequences commonly employed in structural MRI analysis and identify region- and lobar-specific patterns of volume loss and other pertinent imaging findings.
- Recognize the different nuclear medicine imaging agents and the imaging patterns of the most common neurodegenerative diseases.
- Contribute to a multidisciplinary approach in the workup of neurodegenerative disorders.

See rsna.org/learning-center-rg.

Neurodegenerative diseases are a devastating group of disorders that can be difficult to accurately diagnose. Although these disorders are difficult to manage owing to relatively limited treatment options, an early and correct diagnosis can help with managing symptoms and coping with the later stages of these disease processes. Both anatomic structural imaging and physiologic molecular imaging have evolved to a state in which these neurodegenerative processes can be identified relatively early with high accuracy. To determine the underlying disease, the radiologist should understand the different distributions and pathophysiologic processes involved. High-spatial-resolution MRI allows detection of subtle morphologic changes, as well as potential complications and alternate diagnoses, while molecular imaging allows visualization of altered function or abnormal increased or decreased concentration of disease-specific markers. These methodologies are complementary. Appropriate workup and interpretation of diagnostic studies require an integrated, multimodality, multidisciplinary approach. This article reviews the protocols and findings at MRI and nuclear medicine imaging, including with the use of flurodeoxyglucose, amyloid tracers, and dopaminergic transporter imaging (ioflupane). The pathophysiology of some of the major neurodegenerative processes and their clinical presentations are also reviewed; this information is critical to understand how these imaging modalities work, and it aids in the integration of clinical data to help synthesize a final diagnosis. Radiologists and nuclear medicine physicians aiming to include the evaluation of neurodegenerative diseases in their practice should be aware of and familiar with the multiple imaging modalities available and how using these modalities is essential in the multidisciplinary management of patients with neurodegenerative diseases.

Introduction

Neurodegenerative diseases are a collection of diverse, devastating, and increasingly common processes that can cause significant distress and expense. The most common of these, Alzheimer disease, is estimated to affect 5.8 million people in the United States, with a projected increase to 14 million by 2050, as per the Alzheimer's Association (1). In 2019, the cost to the nation from Alzheimer disease and other dementias is estimated to be $290 billion. Although different forms of management exist for these disease processes, treatment efficacy relies on early diagnosis, and overall prognosis remains poor. Diagnosis relies heavily on constellations of clinical findings, which can be difficult to detect and nonspecific. Moreover, patients are typically diagnosed later in the disease process (2), and many patients and families have difficulty accepting or identifying these diagnoses on clinical grounds. Definitive

TEACHING POINTS

- It is important to perform a high-spatial-resolution volumetric T1-weighted sequence with multiplanar reformation and a T2-weighted coronal sequence. The T2-weighted coronal sequence should be performed perpendicular to the long axis of the hippocampus for evaluation of the mesial temporal lobe.
- Although lack of functioning is nonspecific, it can show the distribution of metabolic derangements, which allows differentiation of disease processes in the same manner as that of structural MRI. FDG PET and MRI are useful when used in conjunction to confirm findings and potentially identify early abnormalities that have not yet manifested in structural change.
- At β-amyloid imaging, areas of increased cortical uptake are considered abnormal and correspond to cortical deposition of β-amyloid plaques. An internal control is used to establish a normal uptake pattern, with the cerebellum typically used to compare gray-white differentiation, as the cerebellum rarely has abnormal amyloid accumulation.
- The typical pattern of hypometabolic activity in Alzheimer disease on ^{18}F-FDG PET images involves the parietotemporal region, precuneus, and posterior cingulate gyrus, with sparing of the sensorimotor strips and occipital region, which usually corresponds to the atrophic changes depicted on structural images.
- In patients with DLB, ^{18}F-FDG PET images show asymmetric decreased activity in the frontotemporal lobes similar to that depicted in Alzheimer disease. However, there is preserved metabolism of the posterior cingulate cortex, resulting in the so-called cingulate island sign. Alzheimer disease almost invariably involves the posterior cingulate gyrus, and this is a useful differentiating factor. There is hypometabolism of the occipital lobes, which is helpful to differentiate DLB from typical Alzheimer disease.

objective diagnosis is only possible through brain biopsy or autopsy analysis.

Neuroimaging is advancing to a state in which accurate and objective diagnosis and evaluation of these neurodegenerative disorders is possible. The common availability of high-spatial-resolution MRI has made detailed analysis of sometimes relatively subtle structural changes possible, and the implementation of pathophysiology-specific radiotracers in nuclear medicine allows visualization of the underlying mechanisms of these disease processes. The radiologic and nuclear medicine modalities are complementary, and by using an integrated approach with the clinical presentation, early diagnosis can be achieved, giving patients and families an opportunity to confront the disease and start earlier management.

Structural Imaging

Traditionally the role of neuroimaging in dementia has been to exclude other possible causes that result in cognitive impairment, such as intracranial hemorrhage or space-occupying lesions (Fig 1). Widespread availability and recent advances have expanded the role of structural imaging in the assessment of neurodegenerative disorders. Structural imaging can support the clinical diagnosis of dementia and mild cognitive impairment, and many trials are investigating its value as a marker for disease progression and as outcome measures for disease-modifying treatments (3).

Knowledge of the relevant anatomic structures is a prerequisite to performing structural assessment. Often, the initial step is to assess for global cerebral and cerebellar volume loss. This should be followed by a more in-depth assessment for region- or lobar-specific patterns of volume loss, as these patterns are critical in differentiating the neurodegenerative diseases. Many of the structures in the limbic system, such as the hippocampus and entorhinal cortex (important for memory function), are directly involved in the common neurodegenerative disorders and are vital to interpreting anatomic imaging (4). Another important area to evaluate is the precuneus (medial parietal lobe), which is best evaluated on sagittal T1-weighted MR images (Fig 2). Detection of precuneus involvement also has potential implications in early-onset Alzheimer disease (6).

In routine clinical practice, the assessment is usually qualitative, which may lead to ambiguity and interobserver variability. A few quick, reproducible, and cost-effective semiquantitative scales have been described, particularly for Alzheimer disease, such as the medial temporal atrophy scale by Scheltens et al (7,8) on which patients are scored on the basis of hippocampal formation and the surrounding cerebrospinal fluid spaces. Urs et al (9) expanded on this and described the visual rating system, a system in which patients are scored of the basis of the degree of atrophy of the hippocampus, entorhinal cortex, and perirhinal cortex (Fig 3) (9). Specialized software programs that can provide volumetric analysis are also available for quantitative assessment.

When evaluating patients with suspected dementia at our institution, we perform routine MRI brain sequences, including diffusion-weighted imaging, to help identify infarcts and hypercellular lesions; susceptibility-weighted imaging to identify blood products; and T2-weighted fluid-attenuated inversion-recovery (FLAIR) imaging to identify edema, encephalomalacia, and white matter changes. It is important to perform a high-spatial-resolution volumetric T1-weighted sequence with multiplanar reformation and a T2-weighted coronal sequence. The T2-weighted coronal sequence should be performed perpendicular to the long axis of the hippocampus for evaluation of the mesial temporal lobe (Fig 4) (10).

Other neurodegenerative disorders such as vascular dementia, normal pressure hydrocephalus, Creutzfeldt–Jakob disease, and multiple system

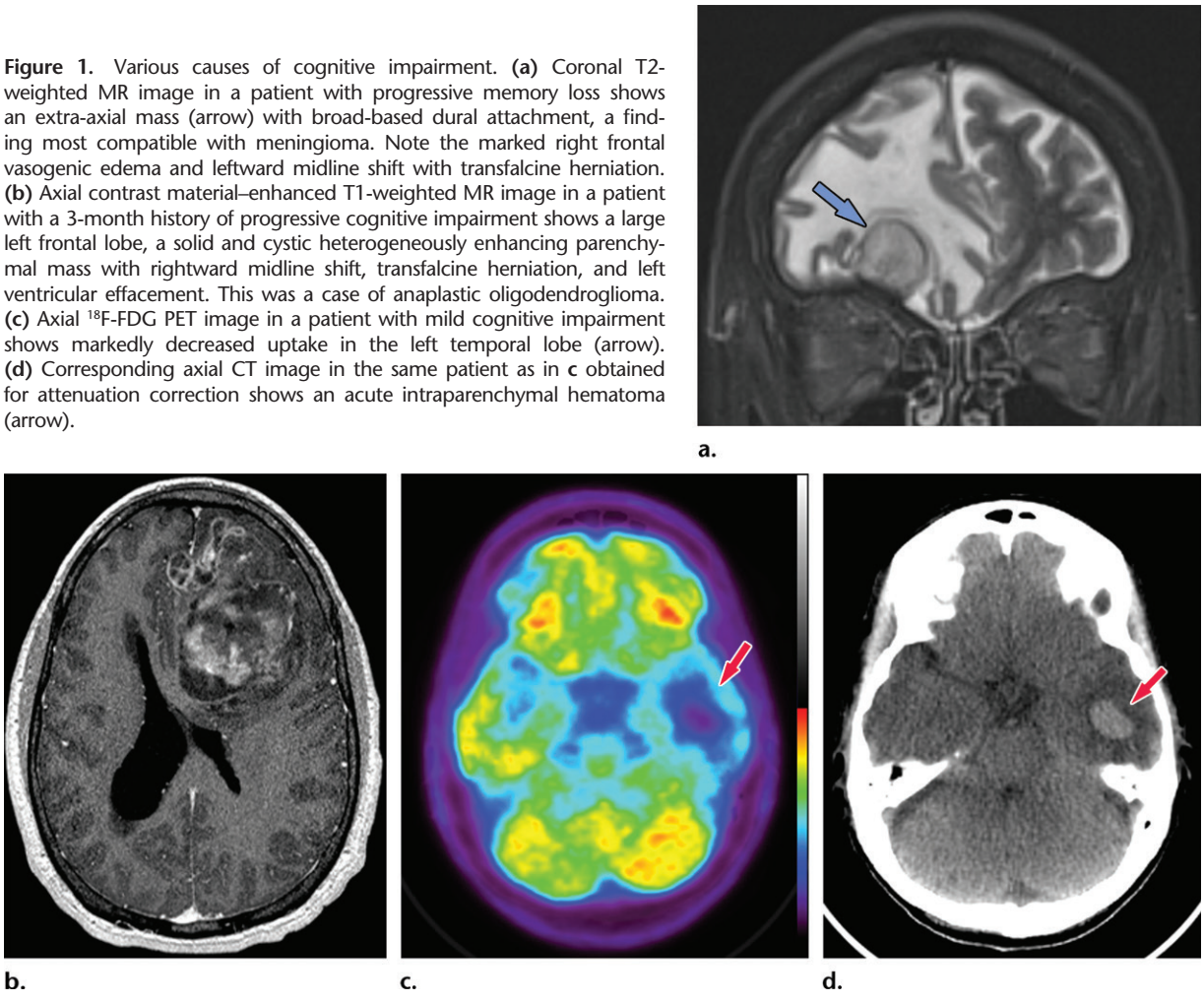

Figure 1. Various causes of cognitive impairment. **(a)** Coronal T2-weighted MR image in a patient with progressive memory loss shows an extra-axial mass (arrow) with broad-based dural attachment, a finding most compatible with meningioma. Note the marked right frontal vasogenic edema and leftward midline shift with transfalcine herniation. **(b)** Axial contrast material–enhanced T1-weighted MR image in a patient with a 3-month history of progressive cognitive impairment shows a large left frontal lobe, a solid and cystic heterogeneously enhancing parenchymal mass with rightward midline shift, transfalcine herniation, and left ventricular effacement. This was a case of anaplastic oligodendroglioma. **(c)** Axial ^{18}F-FDG PET image in a patient with mild cognitive impairment shows markedly decreased uptake in the left temporal lobe (arrow). **(d)** Corresponding axial CT image in the same patient as in **c** obtained for attenuation correction shows an acute intraparenchymal hematoma (arrow).

atrophy, which are discussed in the following sections, can be corroborated at structural imaging.

Molecular Imaging

Multiple nuclear medicine imaging agents exist for neurodegenerative processes, the major ones including PET with fluorine 18 (^{18}F) fluorodeoxyglucose (FDG) and amyloid-β and SPECT with iodine 123 (^{123}I) ioflupane. Additional new agents are under development, including τ-based PET for imaging tauopathies.

FDG PET

FDG is by far the most common contrast agent used in modern PET. The positron-emitting ^{18}F substitutes a hydroxyl group on normal glucose, resulting in a molecule that is taken up by standard glucose transporters. This molecule is then phosphorylated and trapped in cells, resulting in accumulation in metabolically active cells. This creates the metabolism map that is most commonly used in oncologic PET. Additionally, as the brain is almost entirely glucose dependent and metabolically active, it allows visualization of the functioning cerebral cortex. Although this obscures evaluation when looking for metastatic disease, it can be used to visualize areas that are either hyper- or hypofunctioning.

In neurodegenerative diseases, the underlying pathophysiology causes damage to cerebral tissues and alters their normal metabolism. In structural imaging, this causes visible atrophy once enough damage has been done. As FDG allows visualization of metabolic derangement, it can demonstrate areas that are not functioning properly (Fig 5). Although lack of functioning is nonspecific, it can show the distribution of metabolic derangements, which allows differentiation of disease processes in the same manner as that of structural MRI. FDG PET and MRI are useful when used in conjunction to confirm findings and potentially identify early abnormalities that have not yet manifested in structural change (11).

The imaging protocol shares some similarities with traditional oncologic PET, and guidelines adapted from the Society of Nuclear Medicine and Molecular Imaging (SNMMI) procedure standards can be found in Table 1 (12). Similar fasting and dietary restrictions are necessary with monitoring of blood glucose levels on the day of

Figure 2. Pertinent anatomy in structural imaging. **(a)** Sagittal illustration (left) and sagittal correlative T1-weighted MR image (right) show the pertinent anatomy. Attention should be paid to the parietal lobe on parasagittal images, as this is the location of the precuneus that is typically affected in Alzheimer disease. **(b)** Small-field-of-view coronal-oblique T2-weighted MR image with labels, obtained perpendicular to the long axis of the hippocampus for assessment of the mesial temporal lobe, shows additional pertinent structures. Specifically, the visual rating system for mesial temporal atrophy score should be assessed at a plane at the level of the mammillary bodies (5).

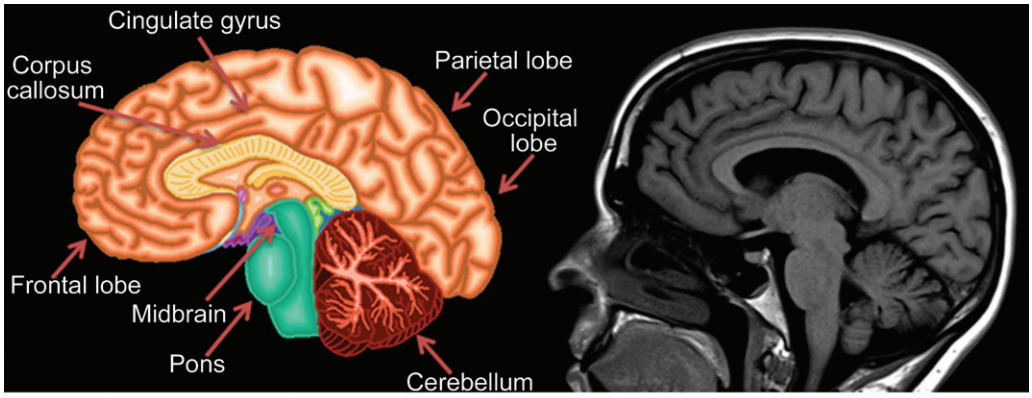

a.

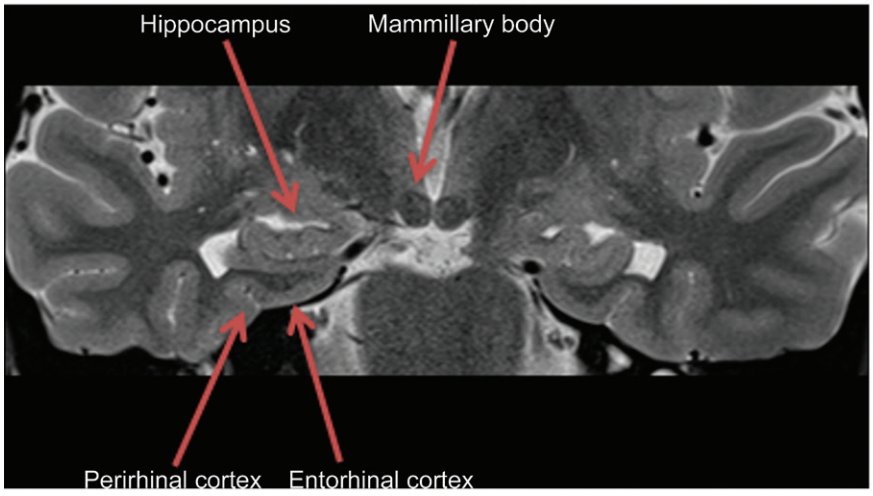

b.

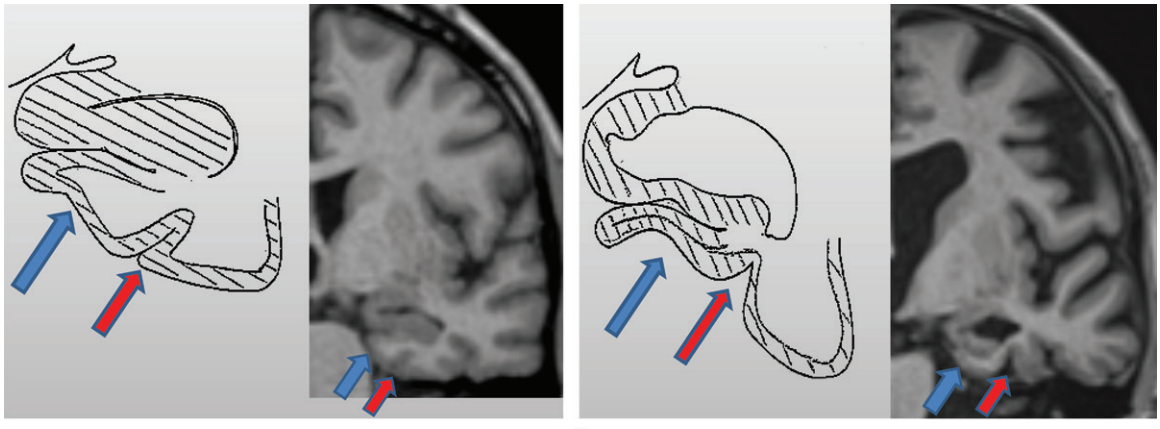

a. **b.**

Figure 3. Mesial temporal lobe assessment. Diagonal lines = gray matter of the cortex. **(a)** Illustration (left) and coned-down coronal T1-weighted MR image (right) obtained for the assessment of mesial temporal atrophy show normal entorhinal cortex (blue arrows), hippocampus, and perirhinal cortex (red arrows) volumes. **(b)** Corresponding illustration (left) and MR image (right) in a patient with clinical mild cognitive impairment shows moderate to severe atrophy of the entorhinal cortex (blue arrows) and hippocampus and moderate atrophy of the perirhinal cortex (red arrows).

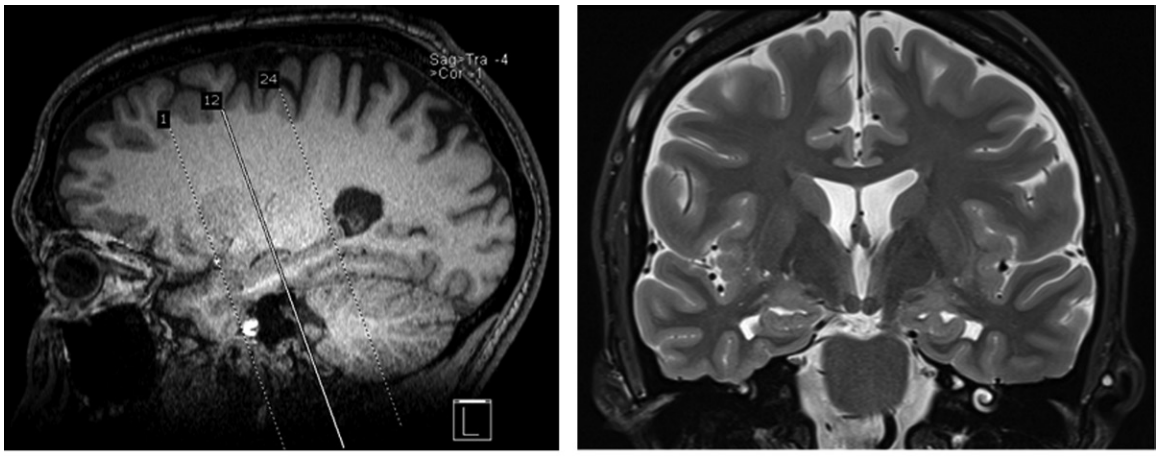

a. b.

Figure 4. Recommended imaging sequences and acquisition. Sagittal high-spatial-resolution T1-weighted MR image **(a)** shows the appropriate prescription (dotted lines), perpendicular to the long axis of the hippocampus, for obtaining the coronal-oblique T2-weighted MR image **(b)**, which is recommended for the assessment of the mesial temporal lobe (10). Solid line in **a** = section from which image **b** was prescribed.

Figure 5. FDG PET images with normal and abnormal findings. **(a)** Axial FDG PET image in a patient without dementia shows a high level of cortical uptake throughout the brain. **(b)** Axial FDG PET image in a patient with advanced Alzheimer disease shows severe cortical hypometabolism involving both the frontal and parietal lobes. Note the relative sparing of the sensorimotor cortices (arrows), which is a classic finding of Alzheimer disease.

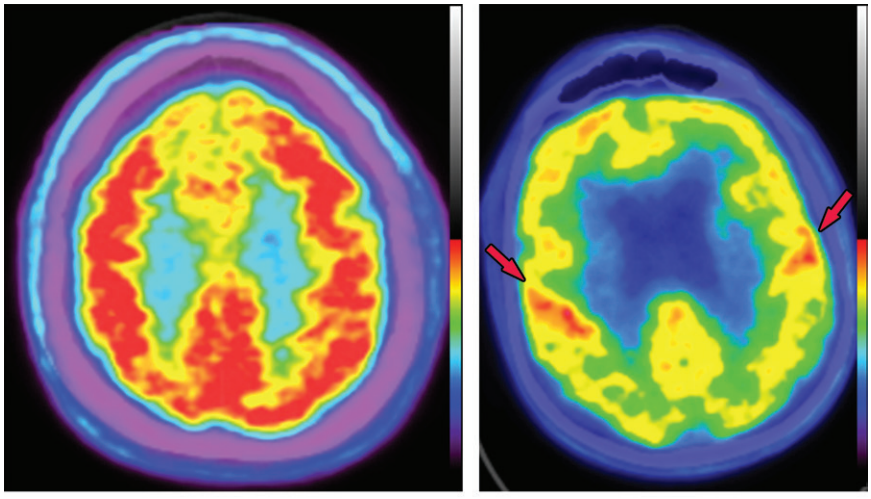

a. **b.**

the examination. In addition to activity limitation and environmental control after injection, patients must have little to no external stimuli to avoid activation of different areas of the cerebral cortex. For example, at our institution patients are typically given eye covers (similar to those used for sleeping on flights) to avoid occipital lobe stimulation.

Amyloid-β PET

A relatively new group of contrast agents exists that allows visualization of abnormal amyloid aggregation. Although the original agent was carbon 11–Pittsburgh compound B, the current major radiopharmaceuticals in this group are all tagged with ^{18}F and include ^{18}F-florbetapir, ^{18}F-florbetaben, and ^{18}F-flutemetamol. These are now commercially available under the names Amyvid (Eli Lilly, Indianapolis, Ind), NeuraCeq (Piramal Group, Mumbai, India), and Vizamyl (GE Healthcare, Chicago, Ill), respectively. A similar mechanism is responsible for the distribution of these agents, wherein the molecules bind to β-amyloid fibrils and plaques. These agents are fairly nonspecific and will also bind to other amyloid deposits, with research being conducted on the clinical utility of working up systemic amyloidosis (13).

At neurologic imaging, normal white matter takes up these agents. The mechanism is not well understood, but research suggests it may bind to myelin-binding proteins and could be used in the workup of demyelinating diseases (14). At β-amyloid imaging, areas of increased cortical uptake are considered abnormal and correspond to cortical deposition of β-amyloid plaques. An internal control is used to establish a normal uptake pattern, with the cerebellum typically used to compare gray-white differentiation, as the cerebellum rarely has abnormal amyloid accumu-

Table 1. SNMMI Recommendations and Radiopharmaceutical Information for ^{18}F-FDG PET

Imaging Parameter	Recommendations
Patient instructions	Fast for 4–6 hours (including no intravenous administration of dextrose or parenteral feeding) Avoid caffeine and alcohol
Preinjection	Check blood glucose levels; levels greater than 150–200 mg/dL may warrant rescheduling Room should be quiet and dimly lit Place intravenous line 10 minutes before injection Minimize patient interaction
Administered activity (adults)	185–740 MBq (5–20 mCi)
Critical organ	Urinary bladder
Effective dose	0.019 mSv/MBq
Image acquisition	Begins 30–60 minutes after injection Examination lasts 5–60 minutes, depending on the injected activity and count statistics Three-dimensional images are commonly obtained (although obtaining two-dimensional images is possible)

Source.—Reference 12.

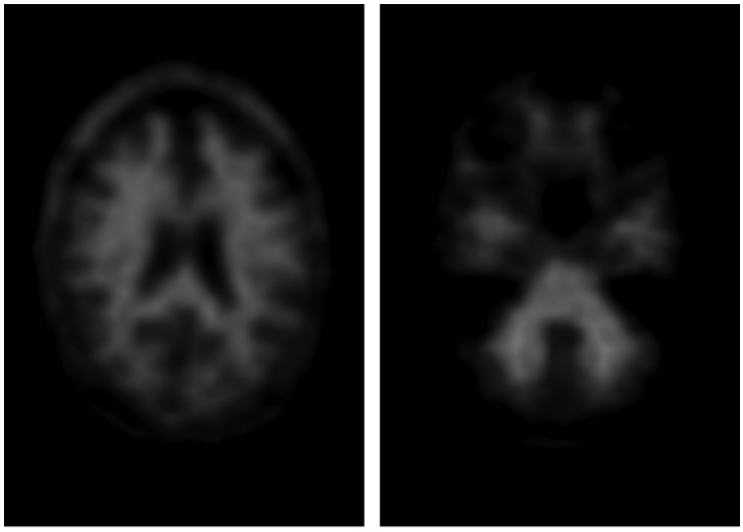

a. b.

Figure 6. Normal amyloid uptake. **(a)** Axial ^{18}F-florbetaben-amyloid PET image shows normal uptake throughout the white matter, with sparing of the cortical gray matter. **(b)** Axial ^{18}F-florbetaben-amyloid PET image shows spared cerebellar gray matter. Gray-white differentiation should be determined by internal control using the axial imaging plane at the level of the cerebellum, as cerebellar gray matter is almost always spared from amyloid deposition, even in advanced cases of dementia.

lation (Fig 6) (15). Although cases with extensive uptake are easily identified, more subtle areas of uptake can be difficult to identify. Also, research has shown that early-phase amyloid imaging can have a distribution similar to that depicted at FDG PET, allowing for metabolic information to be obtained using multiphase imaging (16).

The imaging protocol for amyloid PET is simple, and Table 2 details the guidelines adapted from the SNMMI procedure standards (17). Imaging is performed 30–120 minutes after injection, depending on the dose and radiotracer used, and no special considerations are necessary before injection or during the waiting period.

^{123}I-Ioflupane SPECT

Parkinsonian-type diseases share a similar pathophysiology, with loss of dopaminergic neurons. These neurons are predominantly clustered in the substantia nigra and contain axons that extend into the corpus striatum, with synapses that rely on dopamine to be released to carry out their functions. Dopamine then needs to be collected again by the presynaptic terminal, which uses a transporter called the dopamine transporter (Fig 7). The chosen target for this transporter is ^{123}I-ioflupane, commercially referred to as DaTScan (GE Healthcare). This agent allows visualization of the active synapses in the corpus striatum. Parkinsonian

Table 2: SNMMI Recommendations and Radiopharmaceutical Information for ^{18}F-Amyloid PET

Imaging Parameter	Recommendations
Patient instructions	No special considerations necessary
Preinjection	No special considerations necessary
Administered activity (adults)	^{18}F-florbetapir, 370 MBq (10 mCi) ^{18}F-florbetaben, 300 MBq (8 mCi) ^{18}F-flutemetamol, 185 MBq (5 mCi)
Critical organ	Gallbladder (or large bowel if the patient has undergone cholecystectomy)
Effective dose	Estimated at 4–7 mSv
Image acquisition	^{18}F-florbetapir, 30–50-minute wait, 10-minute examination ^{18}F-flutemetamol, 90-minute wait, 10–20-minute examination ^{18}F-florbetaben, 45–130-minute wait, 20-minute examination Recommended to obtain three-dimensional images

Source.—Reference 17.

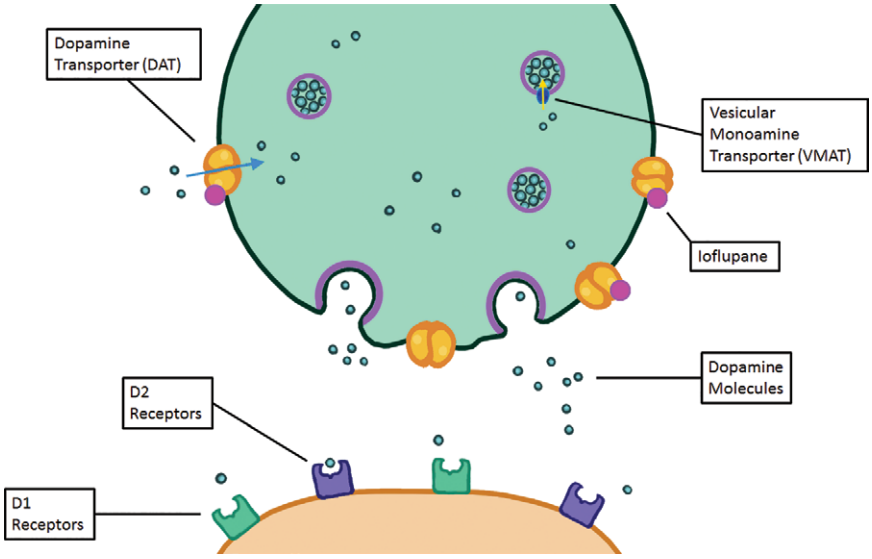

Figure 7. Illustration shows a synapse at a dopaminergic neuron. The green terminal is the presynaptic terminal, and the orange terminal is the postsynaptic terminal. Dopamine molecules are created in the presynaptic neuron and transported into vesicles by vesicular monoamine transporters. These vesicles release the dopamine molecules into the synapse, where the dopamine can then interact with dopamine receptors (*D1* and *D2 receptors*). The dopamine can then either be degraded by catechol-O-methyltransferase (not shown) or taken back up into the presynaptic neuron and recycled through the dopamine transporter. The dopamine transporter is the target of binding, allowing identification of dopaminergic neurons.

diseases cause destruction of dopaminergic neurons, which causes wallerian degeneration of the axons and loss of the dopaminergic synapses, resulting in decreased or absent radiotracer accumulation at the site of these synapses in the corpus striatum. Normal distribution has a comma appearance, with the curved uptake in the caudate heads and putamina. Patients with parkinsonian diseases begin with loss in the putamina, resulting in a period appearance, which can progress to almost complete loss of uptake (Fig 8).

There are a few considerations before beginning ioflupane imaging. Table 3 describes the guidelines adapted from the SNMMI procedure standards (18). Pharmaceuticals with a heavy α-adrenergic effect can severely impair ioflupane binding. Since this agent uses ^{123}I, unwanted radioactivity can accumulate in the thyroid gland. This can be prevented by administering oral iodine or potassium perchlorate to saturate and protect the thyroid.

τ-based PET

One of the newest imaging agents available uses the binding of τ proteins. These agents bind to intra- and extracellular neurofibrillary tangles. Although many are currently in development, the agent with the largest amount of traction was referred to as ^{18}F-AV-1451 during research but now has the name ^{18}F-flortaucipir. These agents have good target-to-background ratios, with healthy patients exhibiting minimal uptake. However, off-target binding can sometimes be depicted in the basal ganglia in otherwise healthy patients (19). The accumulation of a radiotracer should correspond to the pathologic areas of abnormal τ accumulation, such as within the hippocampal body and precuneus in cases of Alzheimer disease. Because of the good target-to-background ratio, even low-level uptake at the mesial temporal lobes and entorhinal cortices can represent early pathologic changes of Alzheimer disease corresponding to Braak stages I and II.

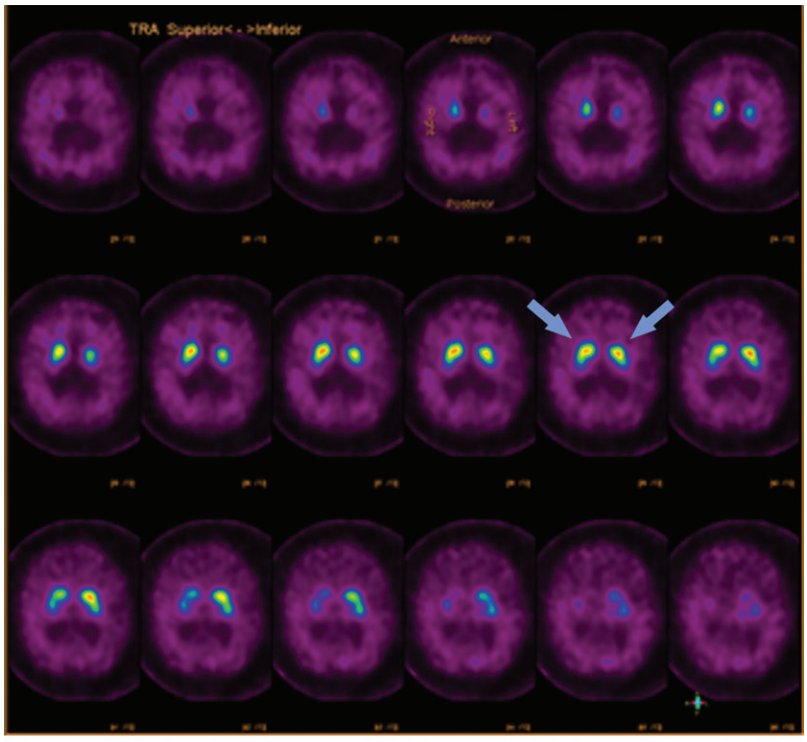

a.

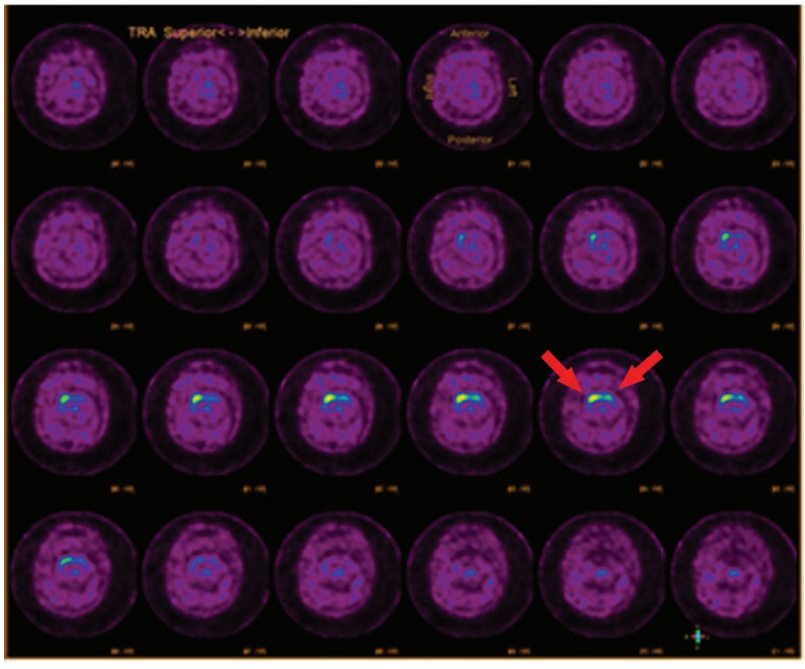

b.

Figure 8. ^{123}I-Ioflupane SPECT images with normal and abnormal findings. **(a)** Axial SPECT images of the brain in a patient without Parkinson disease show bilateral uptake throughout the corpus striatum, with radiotracer uptake in the caudate heads and putamina. This has a comma appearance (arrows) at the appropriate levels. **(b)** Axial SPECT images in a patient with Parkinson disease show overall significantly decreased radiotracer uptake (note the increased image noise), with the most significant loss in the bilateral putamina. Preserved uptake in this case is depicted in the caudate heads, with a period appearance (arrows).

Certain tauopathy-type diseases demonstrate abnormal activity in the affected areas (Fig 9). Tauopathies predominantly accumulate two abnormal types of τ protein, three repeat (3R) and four repeat (4R). Research demonstrates that diseases that accumulate both 3R- and 4R-type misfolded τ proteins result in the most radiotracer accumulation, examples of which include Alzheimer disease, chronic traumatic encephalopathy, and progressive supranuclear palsy (20).

Research also demonstrates that the distribution of radiotracer uptake can also be helpful in differentiating the underlying cause of neurocognitive impairment. For example, while Alzheimer disease demonstrates uptake corresponding to the areas outlined by the Braak staging system, chronic traumatic encephalopathy has been shown to demonstrate diffuse uptake along the gray-white junction related to the underlying cause of chronic injury and shear forces at these locations (21).

Table 3: SNMMI Recommendations and Radiopharmaceutical Information for ^{123}I-Ioflupane SPECT

Imaging Parameter	Recommendations
Patient instructions	Cocaine, amphetamines, methylphenidate, ephedrine, and phentermine should not be used, as these severely reduce ioflupane binding Bupropion, fentanyl, and anesthetic use may also interfere
Preinjection	Administration of a single 400-mg dose of potassium perchlorate, potassium iodide solution, or Lugol solution (equivalent to 100 mg of iodide) 1 hour before tracer injection is recommended to protect the thyroid
Administered activity (adults)	111–185 MBq (3–5 mCi)
Critical organ	Urinary bladder
Effective dose	0.021–0.024 mSv/MBq
Image acquisition	SPECT should start 4–6 hours after injection The interval is recommended to be fixed at an institution to avoid inter- and intrasubject variability Examination time is typically 30–45 minutes (1.5 million total counts)

Source.—Reference 18.

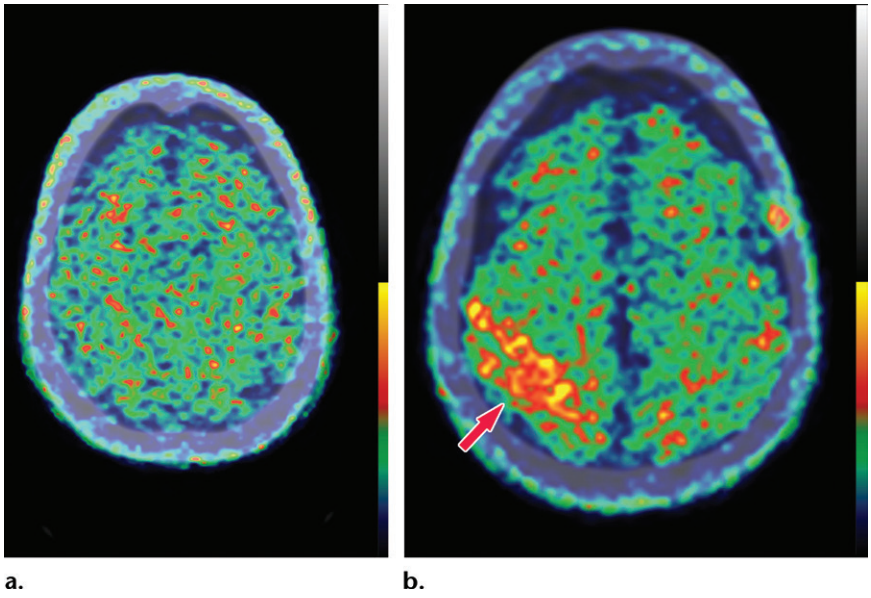

Figure 9. Normal and abnormal findings on τ-PET images. **(a)** Axial ^{18}F-AV-1451 τ-PET image obtained at the convexities shows minimal radiotracer uptake. Additional imaging throughout the brain (not shown) did not show significant focal uptake at any location. **(b)** Axial τ-PET image of a patient with cognitive impairment shows discrete abnormal radiotracer accumulation (arrow) in the right parietal lobe.

Computer-assisted Quantitative Evaluation

In nuclear medicine, quantification of uptake is possible based on the counts in a specific area. Standardized uptake values as used in oncologic PET are difficult to use, and the extensive data required to truly standardize the measurements do not yet exist. However, comparing uptake to that in known normal examinations can allow relative quantitative regional measurements and generate maps corresponding to the standard deviations of uptake from normal examinations. Datasets containing numerous normal examinations are generated, and through machine learning, algorithms are able to learn the normal distribution of uptake. This algorithm can be applied to abnormal cases and generate color maps to visually demonstrate areas that have abnormally decreased uptake that fall outside a specified set of standard deviations below a certain *z* score (Fig 10), in which the *z* score reflects the number of standard deviations from those of normal uptake, similar to that in a dual-energy x-ray absorptiometry examination. This functionality exists in multiple available software packages for both PET and SPECT. This technique can be helpful for identifying subtle areas of abnormality (22), and it can be used in research protocols as a method of quantification for a more regimented comparison.

Pathophysiology of Neurodegenerative Diseases

The various neurodegenerative diseases are characterized by unique disturbances on the histopathologic level. Although the exact mechanisms that result in the development of these diseases are mostly unknown, these entities can be loosely grouped

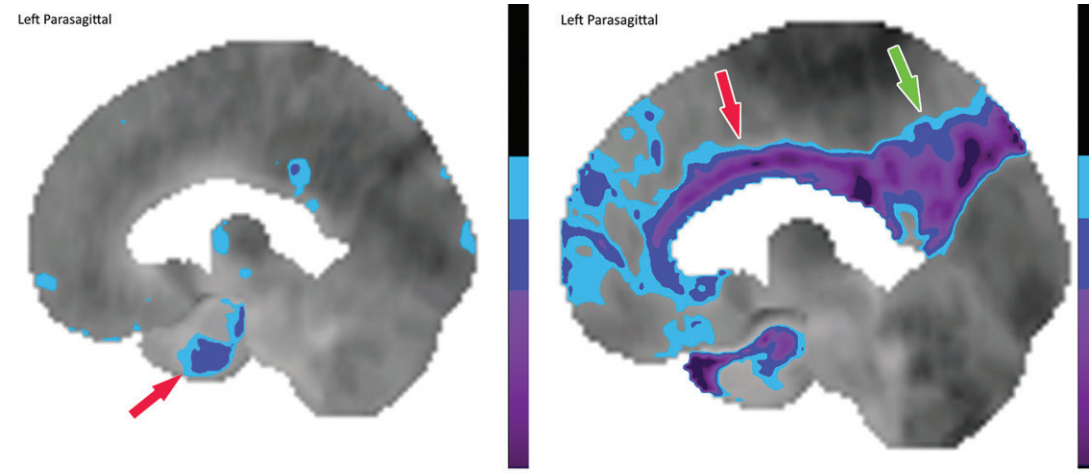

a. b.

Figure 10. Computer-aided quantitation in FDG PET. **(a)** Sagittal color map of the *z* score of FDG uptake in a normal subject shows only minimal decreased uptake at the left mesial temporal lobe (arrow). **(b)** Sagittal color map in a patient with Alzheimer disease shows characteristic markedly decreased uptake along the cingulate gyrus (red arrow) and left precuneus region (green arrow). In these examples, light blue areas represent a *z* score between 1.6 and 2.3 (95–99th percentile), dark blue areas are between 2.3 and 3.1 (99–99.9th percentile), and purple areas are below 3.1 (99.9th percentile) standard deviations from those of normal examinations.

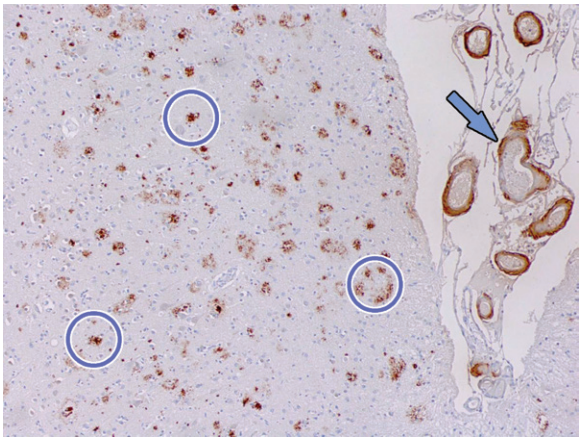

Figure 11. β-amyloid staining. Photomicrograph of the midfrontal cortex with amyloid-β-5 staining in a patient with dementia shows numerous aggregates of extracellular amyloid plaque (circles). Amyloid deposition is also depicted along adjacent vascular walls (arrow). These aggregates are the site of binding of amyloid PET radiotracers. Although the presence of amyloid aggregates is sensitive for the detection of Alzheimer disease, it is not highly specific and can be visualized in Alzheimer disease and certain cases of dementia with Lewy bodies (DLB). The significance of these plaques is still not well understood, and they may be either primary or secondary findings to the underlying disease process.

into categories that share an over-arching similar histopathology. This is imprecise and in some cases there is significant crossover, but recognizing the basis of these changes is essential for understanding which molecular imaging modalities can be applied to which disease. The three that relate the most to imaging are the concept of tauopathies, β-amyloid accumulation, and α-synucleinopathies.

Tauopathies are characterized by the aggregation of misfolded τ proteins. The τ proteins stabilize neural microtubules in the normal brain. When misfolded, they clump and destabilize microtubules, causing dissolution and the formation of neurofibrillary tangles. Entities that fall into this group include frontotemporal lobar degeneration (FTLD), corticobasal degeneration, and progressive supranuclear palsy. As mentioned previously, misfolded proteins come in two main varieties, 3R and 4R isoforms, and different disease processes accumulate different isoforms (20). Interestingly, chronic traumatic encephalopathy also results in the abnormal accumulation of 3R and 4R τ aggregates (23). Alzheimer disease also has 3R and 4R τ aggregates but is considered a secondary tauopathy given the equal or greater representation of β-amyloid accumulation in the disease process (24). These agents can be imaged by τ agents such as ^{18}F-AV-1451 (or ^{18}F-flortaucipir).

β-amyloid accumulation is one of the primary aberrations in patients with Alzheimer disease. Extracellular amyloid plaques are the classic finding (Fig 11), although evidence suggests intracellular amyloid accumulation also plays a role (25). These plaques can be detected by amyloid-specific agents. Although Alzheimer disease is typically the entity defined by amyloid plaques, amyloid accumulation (and therefore abnormal amyloid nuclear imaging) can be depicted in other entities as well (26–28).

Abnormal accumulation of α-synuclein is depicted in cases of neurodegenerative disease with Lewy body inclusions (Fig 12). The diseases making up the α-synucleinopathy subgroup are Parkinson disease, dementia with Lewy bodies (DLB), and multiple system atrophy. Clinically, these entities demonstrate parkinsonian symptoms with

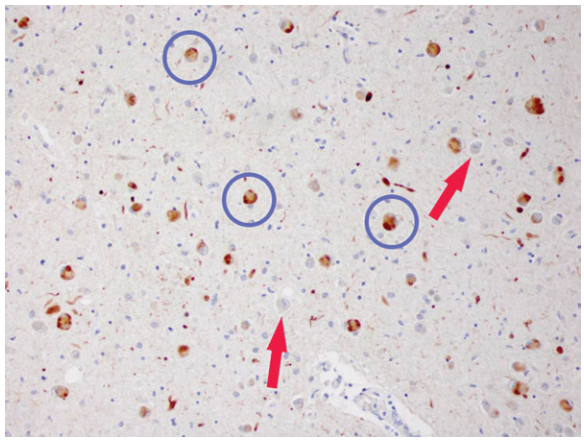

Figure 12. Staining with α-synuclein. Photomicrograph of the amygdala with 81A staining of α-synuclein in a patient with DLB shows numerous intracellular α-synuclein inclusions (circles), referred to as Lewy bodies. Note the appearance of the relatively normal neurons (arrows), which have no visible inclusions. Clinically available radiotracers for α-synuclein do not exist. However, these inclusion bodies are cytotoxic and result in neuronal loss, which is the basis for dopaminergic neuron and synapse loss that can be visualized with ioflupane (dopamine transporter) imaging.

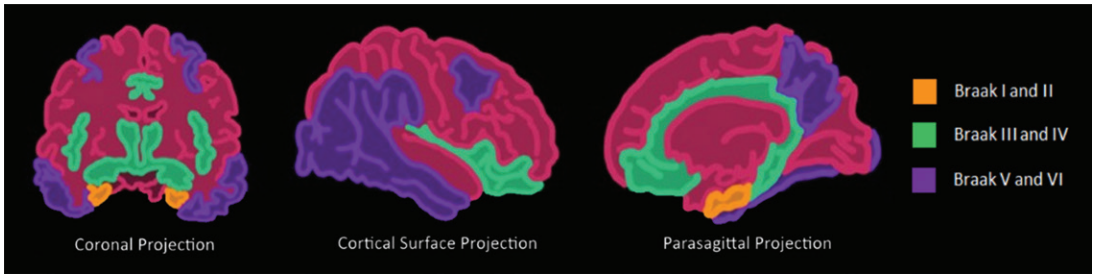

Figure 13. Illustrations show the Braak τ staging system in Alzheimer disease in three different imaging planes. Braak stages I and II (orange areas) are characterized by abnormal τ aggregation at the entorhinal cortex, with early involvement at the hippocampus. Braak stages III and IV (green areas) are characterized by more advanced hippocampal aggregation and further involvement of the limbic system. Braak stages V and VI (purple areas) are characterized by extension into the neocortex, specifically involving the precuneus, temporal lobes, and lingual gyrus. This staging predicts the sequence of findings at structural imaging, FDG PET, and τ-based PET.

damage to the basal ganglia and visual cortices. Because of the damage to the basal ganglia, these are typically abnormal on ^{123}I-ioflupane SPECT images. Of interest, α-synuclein also accumulates in the gastrointestinal tract, resulting in gastrointestinal symptoms (29).

Alzheimer Disease

Alzheimer disease is the prototypical neurodegenerative disease. This is by far the most common neurodegenerative disease, accounting for the majority of patients with dementing disorders. This translates into a total disease incidence of as high as 20 million, with 5 million new diagnoses each year. Per total population, this accounts for nearly 5% of all individuals 65 years of age or older (30). Some estimates are even higher at 6%–10% (31). Annual costs worldwide in 2015 were estimated at over $950 billion, with a cost per patient of $19 000 (32).

Histopathologically, this disease is characterized by the accumulation of β-amyloid plaques and misfolded τ protein neurofibrillary tangles. β-amyloid deposition patterns and the significance of amyloid burden to clinical symptoms is not well understood (33), but τ protein deposition does follow a more predictable pattern, which is classified by the Braak staging system (34). This is broken down into six stages, where stages I and II show uptake at the entorhinal cortex, III and IV are in the limbic system and hippocampus, and V and VI are spread throughout the rest of the cortex (Fig 13). These misfolded τ proteins are a mixture of 3R and 4R isoforms.

Clinically, Alzheimer disease begins as mild cognitive impairment, which slowly progresses to outright dementia. Diagnostic criteria are complex, but generally diagnosis requires an insidious onset (rapid-onset dementia is concerning for other causes, such as Creutzfeldt–Jakob disease), amnesia with loss of short-term recall, language deficits starting with word-finding abnormalities, and loss of spatial orientation. Importantly, these symptoms must be enough to impair daily life (35). The slow onset and capability to compensate contribute to difficulty and delay in diagnosis. Additionally, there are atypical variants that exhibit symptoms more similar to those of FTLD, as discussed in the next section.

The earliest atrophic changes in Alzheimer disease on structural MR images are depicted in the entorhinal cortex (Brodmann area 28), and eventually in the hippocampus (36). The atrophic changes then typically follow a predictable pattern following the pathologic Braak staging

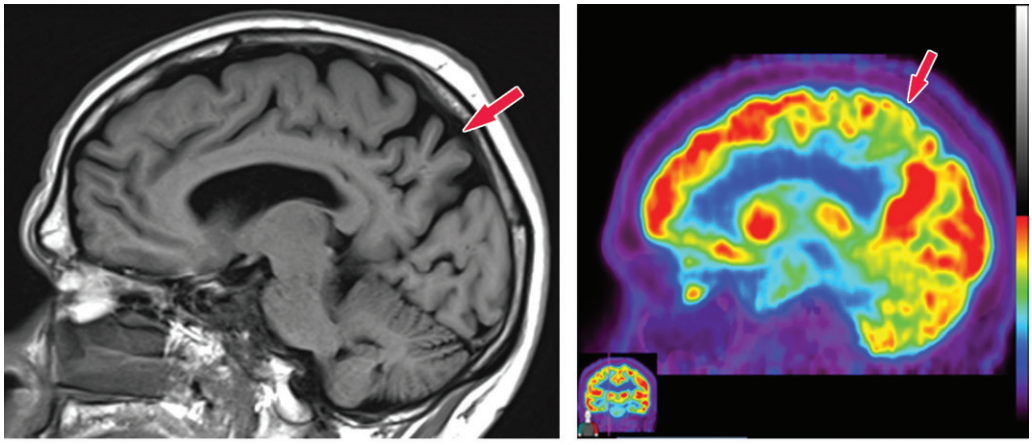

a. b.

Figure 14. Alzheimer disease. **(a)** Sagittal T1-weighted MR image in a patient with memory loss shows disproportionate moderate volume loss in the precuneus (arrow), a finding suspicious for Alzheimer disease. The remainder of the brain parenchymal volume is relatively preserved. **(b)** Sagittal ^{18}F-FDG PET image shows corresponding decreased activity in the precuneus (arrow). Image inset shows a coronal section through the middle of the brain in this particular case to aid in lateralization. Normal uptake is depicted in the frontal and occipital regions, reinforcing the diagnosis of Alzheimer disease.

system involving the neocortex, particularly the precuneus. The typical pattern of hypometabolic activity in Alzheimer disease on ^{18}F-FDG PET images involves the parietotemporal region, precuneus, and posterior cingulate gyrus, with sparing of the sensorimotor strips and occipital region, which usually corresponds to the atrophic changes depicted on structural images (Fig 14). However, in some cases the molecular imaging findings may show advanced hypometabolic activity without region-specific changes at structural imaging (Fig 15). Many Alzheimer disease variants, such as language, visual, and dysexecutive variants, are currently under investigation, and they tend to follow the general distribution as previously described, with few relatively distinct areas of uptake (37).

Amyloid imaging agents show abnormal cortical uptake corresponding to the β-amyloid accumulation. Classic uptake is usually symmetric and diffuse throughout the cortical gray matter, with sparing of the cerebellum, which is used as an internal control (Fig 16). Studies have shown relatively little variation in uptake across Alzheimer disease and its variants, and amyloid accumulation irrespective of the burden may result in increased vulnerability for early-onset Alzheimer disease (38). Although amyloid deposition can be diagnosed in patients without clinical dementia, negative amyloid uptake has a good negative predictive value for Alzheimer disease. The τ imaging agents show uptake distribution following the patterns described in the Braak staging system, which is readily detectable given the overall minimal normal levels of uptake (39).

Dementia with Lewy Bodies

DLB is the second most common primary dementing neurodegenerative disorder after Alzheimer disease. Estimates predict 10%–25% of dementia cases are related to DLB (40). However, it is likely that this specific disorder is underdiagnosed owing to a general lack of awareness and misdiagnosis as traditional Alzheimer disease.

DLB is defined histopathologically by the aggregation of Lewy bodies, which is similar to that which occurs in Parkinson disease. These Lewy bodies are clumps of misfolded α-synuclein proteins, which create inclusions that can be visualized under a microscope. There is a separate Braak staging system for Lewy body aggregation, which was originally described in Parkinson disease. This suggests that Lewy body progression starts peripherally, migrating to the pons and midbrain, then eventually spreading through the supratentorial regions. Because of the spread of involvement, this results in damage to dopaminergic neurons centered at the substantia nigra and basal ganglia (41).

Clinically, DLB is characterized by progressive cognitive decline accompanied by parkinsonian and visual symptoms, frequently visual hallucinations. This is similar to Parkinson disease dementia, which is differentiated from DLB by the order of onset, in which parkinsonism without cognitive decline appears first, followed by dementia (42). Similar to Parkinson disease, there are significant gastrointestinal symptoms, including constipation, nausea, vomiting, and gastroparesis. These symptoms are attributed to Lewy body deposition within enteric neurons throughout the gastrointestinal tract.

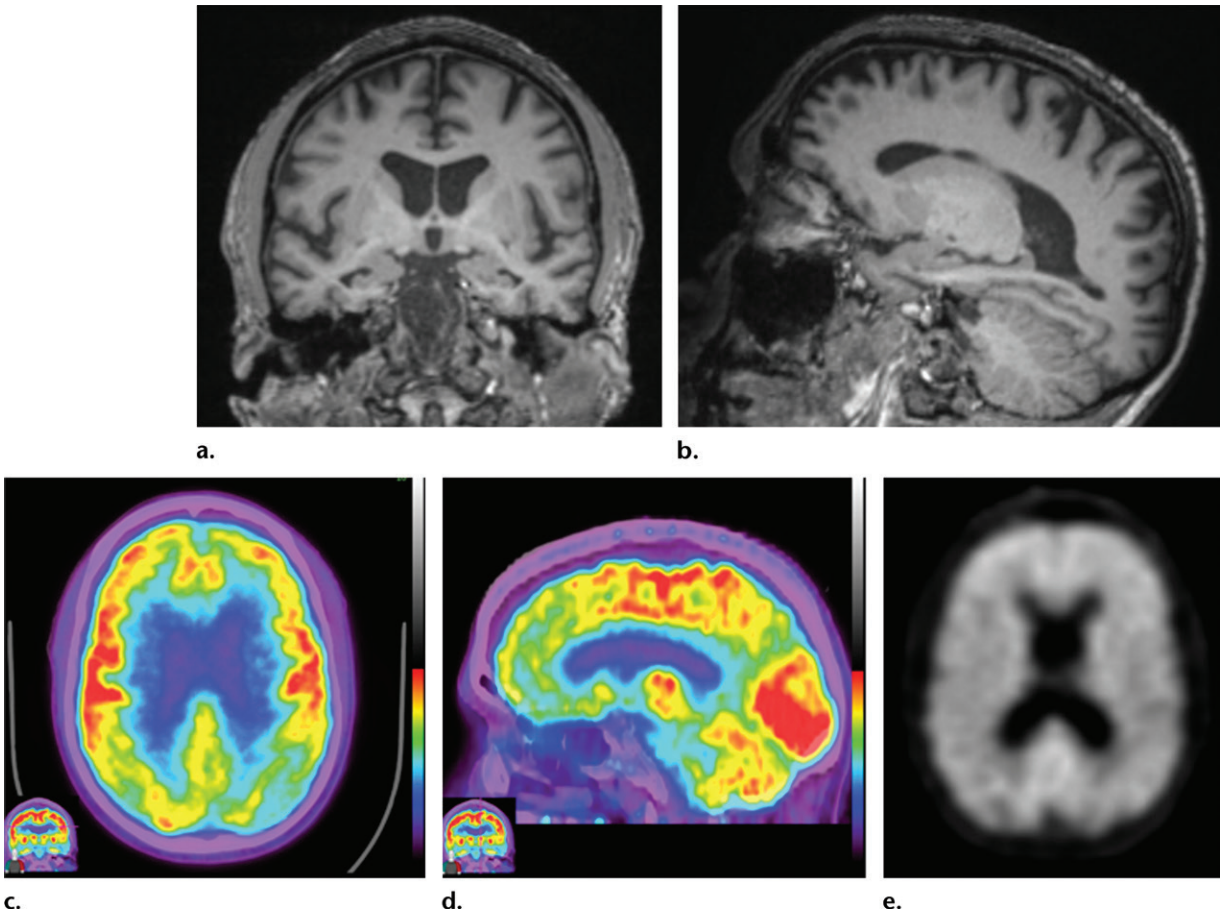

Figure 15. Alzheimer disease. **(a, b)** Coronal **(a)** and sagittal **(b)** T1-weighted MR images in a patient with suspected Alzheimer disease show mild-to-moderate generalized volume loss. **(c, d)** Axial **(c)** and sagittal **(d)** ^{18}F-FDG PET images show markedly decreased activity in the bilateral frontal lobes and precunei. Image insets show a coronal section through the middle of the brain in this particular case to aid in lateralization. **(e)** Axial ^{18}F-florbetaben image shows diffuse cortical uptake, which is a grossly abnormal finding, confirming amyloid deposition. Corroborative imaging findings are supportive of the clinical diagnosis of Alzheimer disease.

Structural imaging findings are less conspicuous and nonspecific in DLB compared with those of Alzheimer disease and FTLD. There is relative preservation of the mesial temporal lobe and less severe atrophy of the hippocampus compared with those of Alzheimer disease (42). Additionally, the swallow tail sign has been described for the normal appearance of nigrosome 1 in the substantia nigra on axial high-spatial-resolution susceptibility-weighted images. Nigrosome 1 demonstrates high signal intensity on axial susceptibility-weighted images and is surrounded by low signal intensity, resembling a swallow's tail. Absence of the normal high signal intensity (absent swallow tail sign) is reported to have high diagnostic utility in parkinsonian neurodegenerative diseases and can be supportive of a DLB diagnosis (43). In patients with DLB, ^{18}F-FDG PET images show asymmetric decreased activity in the frontotemporal lobes similar to that depicted in Alzheimer disease; however, there is preserved metabolism of the posterior cingulate cortex, resulting in the so-called cingulate island sign (Fig 17). Alzheimer disease almost invariably involves the posterior cingulate gyrus, and this is a useful differentiating factor (44). There is hypometabolism of the occipital lobes, which is helpful to differentiate DLB from typical Alzheimer disease.

^{123}I-ioflupane SPECT images will show decreased striatal uptake in DLB, beginning in the putamen and resulting in a period appearance with sparing of the caudate head (Fig 18), in contradistinction to that in healthy patients and patients with Alzheimer disease, in which there is a comma appearance of the normal striatal uptake. This can be asymmetric and later in the disease can progress to also involve the caudate head. This can be helpful to corroborate findings depicted on MR and FDG PET images.

Unfortunately, β-amyloid imaging may not adequately differentiate DLB from Alzheimer disease, as many cases may exhibit significant abnormal β-amyloid accumulation. However, Parkinson disease dementia has been shown to exhibit lower levels of abnormal β-amyloid

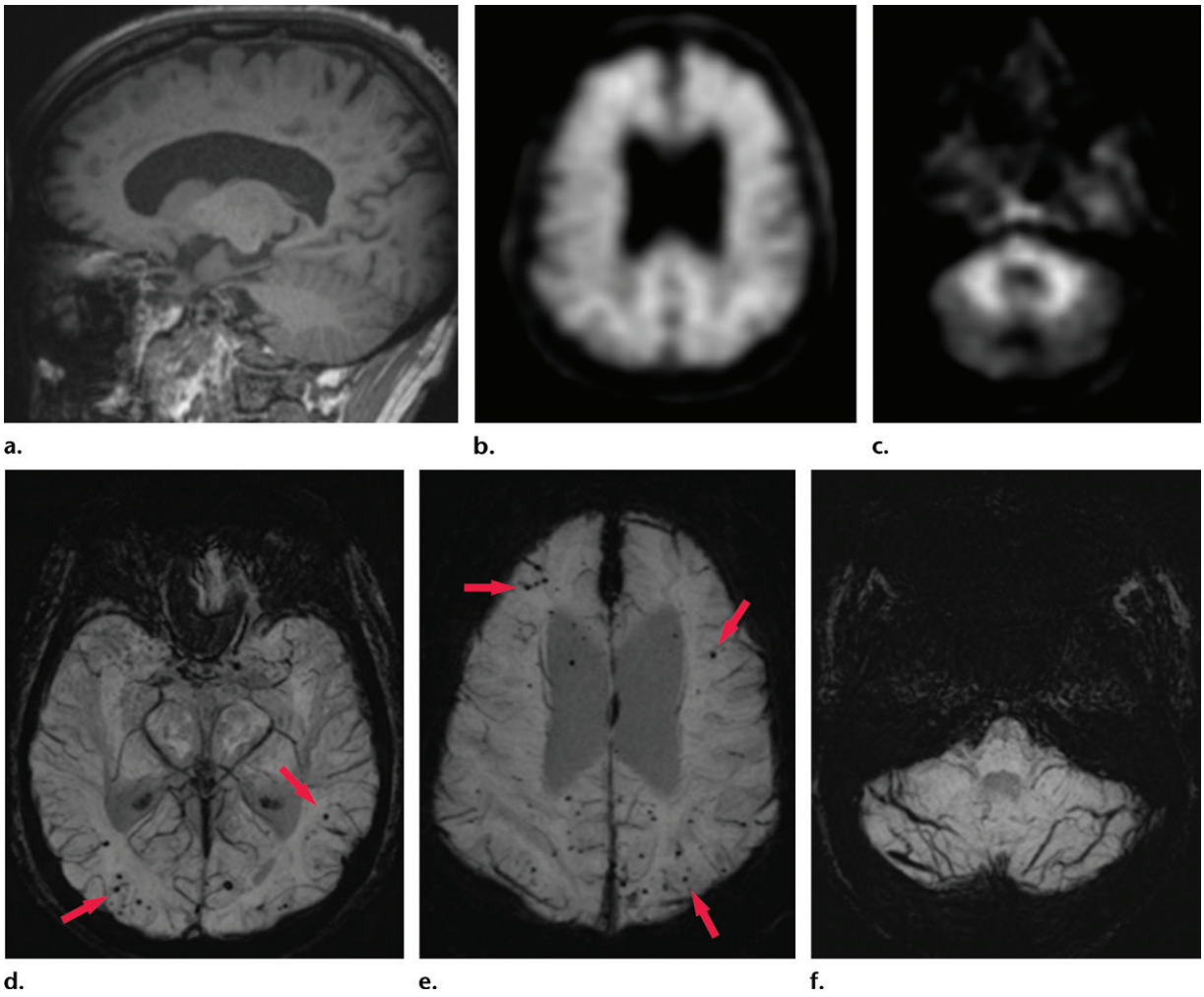

Figure 16. Patient with memory loss. **(a)** Sagittal T1-weighted MR image in a patient with memory loss shows relatively preserved cortical volume. **(b)** Axial ^{18}F-florbetaben image at the level of the lateral ventricles shows diffuse abnormal uptake, confirming amyloid deposition. **(c)** Axial image at the level of the cerebellum shows preserved gray-white differentiation. **(d, e)** Axial susceptibility-weighted minimum intensity projection images at the level of the atria **(d)** and body **(e)** of the lateral ventricles show multiple areas of round signal void (arrows) scattered throughout the periphery of the cortices, compatible with cerebral amyloid angiopathy. **(f)** Axial susceptibility-weighted minimum intensity projection image at the level of the cerebellum shows the lack of abnormal susceptibility in the cerebellum, compatible with the sparing noted at amyloid PET imaging. This case highlights the complementary role of structural and molecular imaging with findings compatible with Alzheimer disease and cerebral amyloid angiopathy.

uptake (26,27). Neither DLB nor Parkinson disease dementia should have definite abnormal uptake at ^{18}F-AV-1451 τ-based imaging in a Braak staging system–type distribution.

Frontotemporal Lobar Degeneration

FTLD is a term applied to a number of similar tauopathies that result in destruction of the frontal and temporal lobes. The entity referred to as *Pick disease* falls into this category. Once thought of as rare entities, these diseases appear to have a higher prevalence than was previously assumed (45,46). This is likely due to increased awareness and improved diagnostic criteria. Alzheimer disease and DLB are accepted as having a higher overall prevalence, with this group representing the third most common group of dementing disorders in patients over 65 years of age and the second most common group in patients under 65 years of age (47).

The histopathology of these diseases demonstrates the accumulation of abnormal τ proteins in the affected areas. Depending on the subtype, different isoforms of the τ protein are involved, with most entities having either a predominant 3R- or 4R-type isoform. Although the classic Pick disease has Pick bodies, many of the other subtypes do not demonstrate this typical appearance (48).

The clinical presentation is divided into two main groups: behavioral-variant frontotemporal dementia (bvFTD) and primary progressive aphasia (PPA). All forms of frontotemporal dementia have both marked behavioral changes

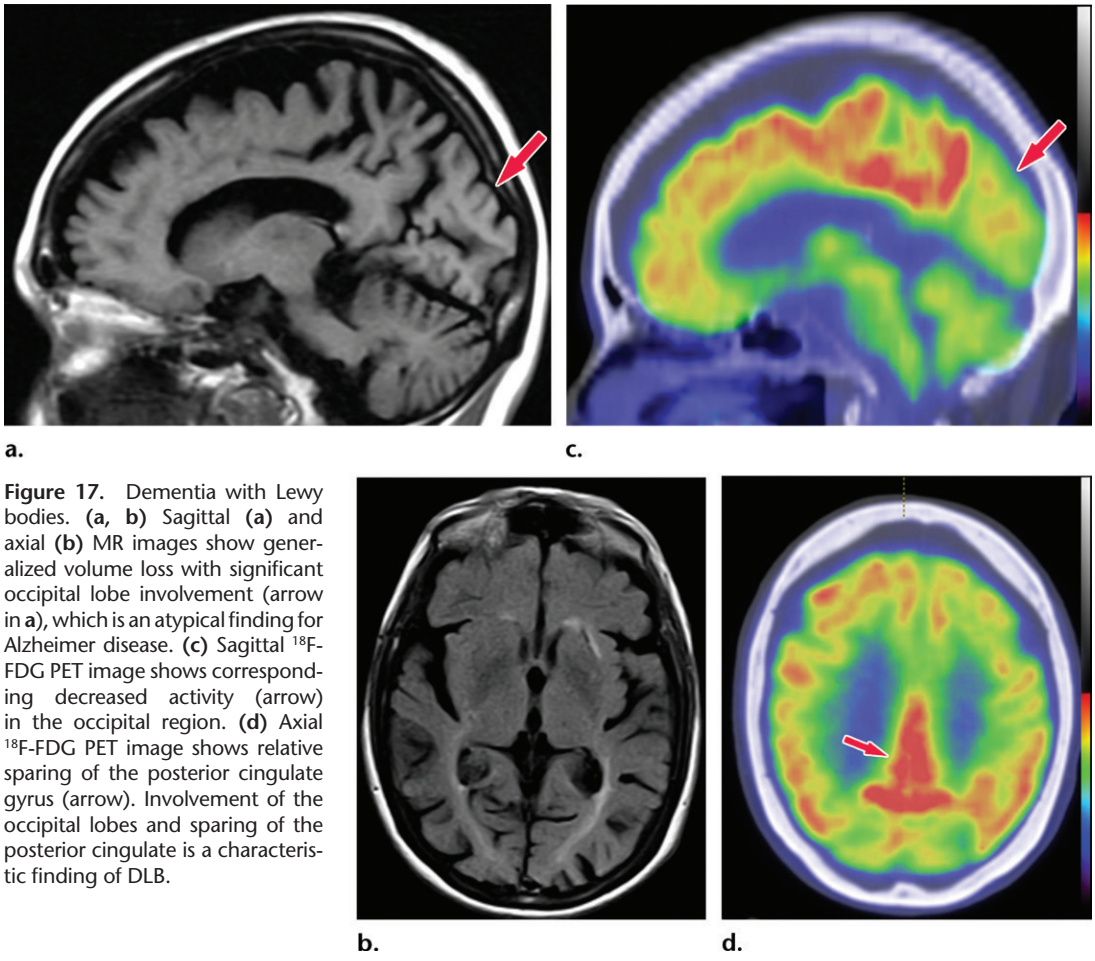

Figure 17. Dementia with Lewy bodies. **(a, b)** Sagittal **(a)** and axial **(b)** MR images show generalized volume loss with significant occipital lobe involvement (arrow in **a**), which is an atypical finding for Alzheimer disease. **(c)** Sagittal ^{18}F-FDG PET image shows corresponding decreased activity (arrow) in the occipital region. **(d)** Axial ^{18}F-FDG PET image shows relative sparing of the posterior cingulate gyrus (arrow). Involvement of the occipital lobes and sparing of the posterior cingulate is a characteristic finding of DLB.

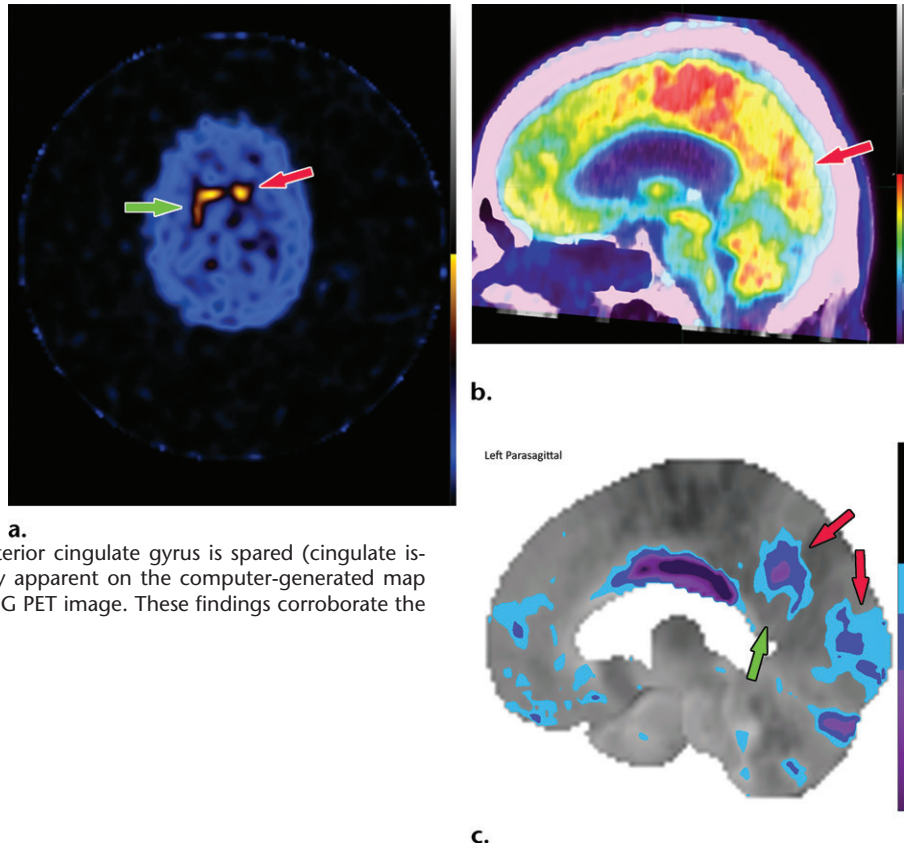

Figure 18. Dementia with Lewy bodies. **(a)** Axial ^{123}I-ioflupane SPECT image in a patient with memory loss shows decreased left striatal uptake with a period appearance (red arrow), confirmatory of a parkinsonian neurodegenerative disease. Note the normal right striatal uptake with a comma appearance (green arrow), representing preserved putaminal uptake. **(b)** Sagittal ^{18}F-FDG PET image shows subtle decreased uptake within the occipital region (arrow). **(c)** Parasagittal computer-generated map shows a statistically significant decrease in FDG uptake in the precuneus and occipital lobe (red arrows). Note that the posterior cingulate gyrus is spared (cingulate island sign), which is more readily apparent on the computer-generated map (green arrow) than on the ^{18}F-FDG PET image. These findings corroborate the diagnosis of DLB.

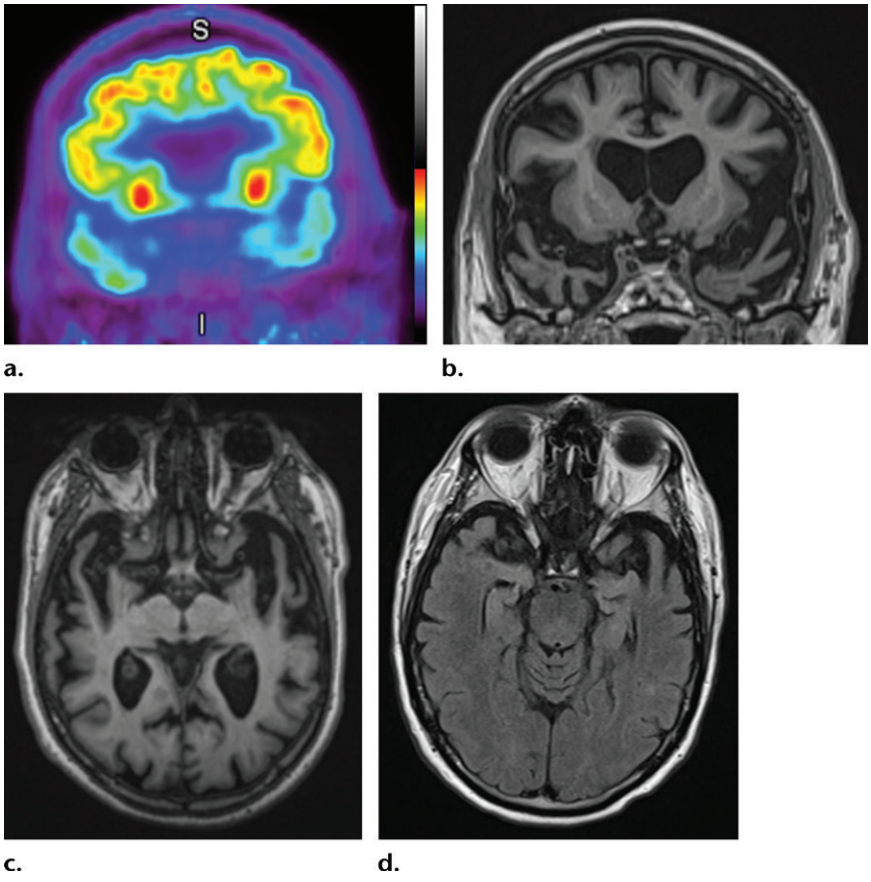

Figure 19. Frontotemporal lobar degeneration. **(a)** Coronal ^{18}F-FDG PET image at the level of the anterior temporal lobes shows markedly decreased temporal lobe uptake. *I* = inferior, *S* = superior. **(b, c)** Coronal **(b)** and axial **(c)** T1-weighted MR images show severe bilateral temporal lobe atrophy. **(d)** Axial MR image at the level of the temporal lobes obtained 5 years earlier demonstrates the significant progressive atrophy in this patient.

and decrease in overall cognitive function. The bvFTD type is characterized by marked behavioral changes as the first and most clinically obvious symptoms. PPA is defined by difficulties in language function with three main variants: semantic variant (impaired naming and comprehension), nonfluent variant (halting, interrupted speech), and logopenic variant (impaired word retrieval with word-finding pauses) (47).

Most research into the use of structural imaging for FTLD has been aimed at improving differentiation from other neurodegenerative disorders and differentiating between the subtypes (49). All the subtypes show predominant frontotemporal atrophy (Fig 19), with the severely affected regions showing knifelike gyri owing to the marked loss of brain volume. There is relative sparing of the parietal and occipital lobes. In bvFTD, there is volume loss in the frontal and temporal lobes, with asymmetric involvement of the anterior temporal lobes, prefrontal cortices, the insula, anterior cingulate, striatum, and thalamus (50). In PPA, there is asymmetric anteroinferior temporal lobe atrophy, with left-sided atrophy more common than the right (51).

The typical pattern of hypometabolic activity on ^{18}F-FDG PET images usually follows the structural changes and shows asymmetric decreased activity in the frontal and temporal lobes. Classically, there is comparative sparing of the precuneus and occipital lobes, differentiating FTLD from Alzheimer disease and DLB (Fig 20).

β-amyloid PET can be used to differentiate between Alzheimer disease and FTLD, as amyloid deposition is not part of the FTLD spectrum. A few studies have shown amyloid positivity in FTLD, which may be secondary to false-positive results, coexistent FTLD and Alzheimer pathology, and atypical variants of Alzheimer disease mimicking FTLD (52).

The role of τ imaging is unclear at this time. ^{18}F-AV-1451 appears to be relatively insensitive to FTLD, as most of these entities are not a mixture of 3R and 4R (20). However, there are multiple other τ candidates being developed, and further research is necessary to assess their utility in FTLD.

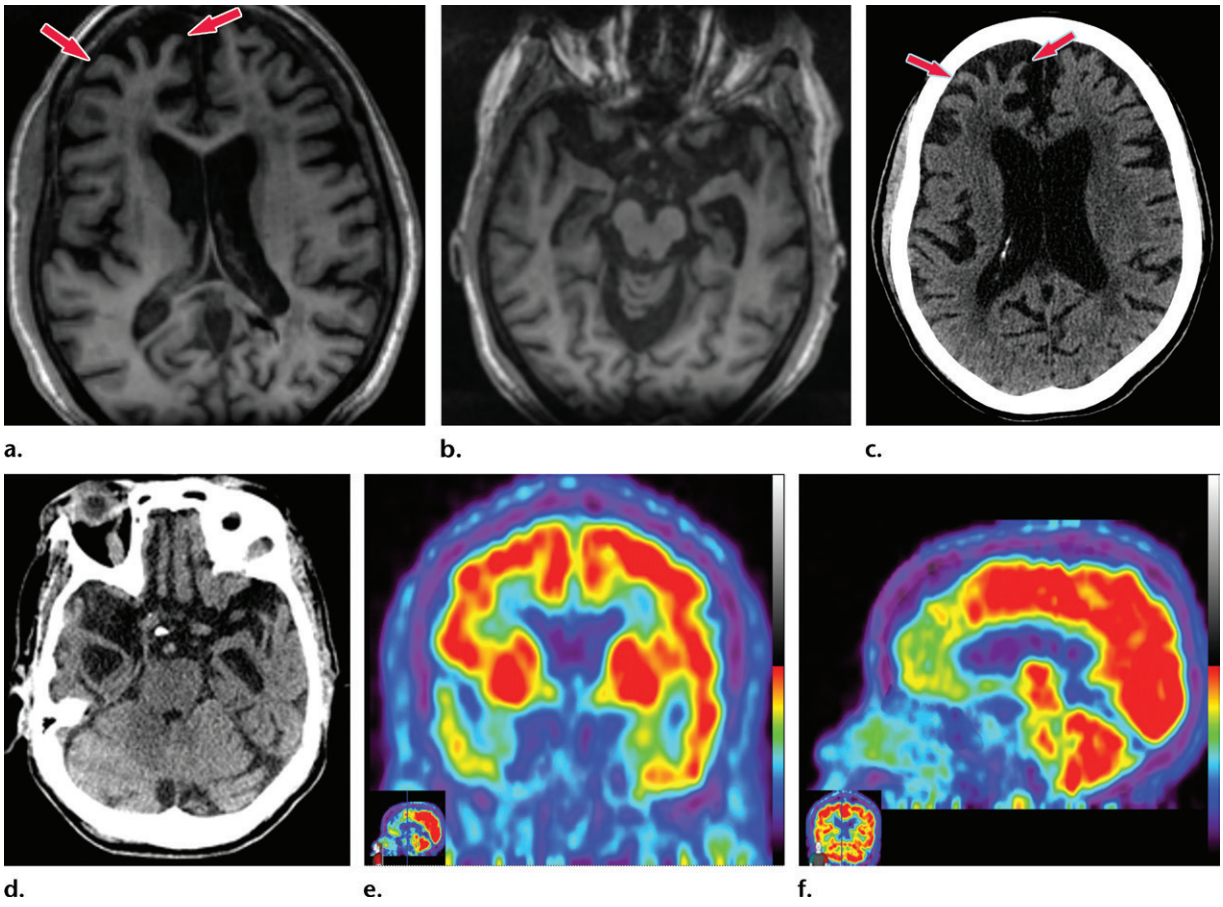

Figure 20. Frontotemporal lobar degeneration. **(a, b)** Axial T1-weighted MR images at the convexities **(a)** and temporal lobes **(b)** show moderate frontotemporal atrophy. Note the atrophy at the right frontal lobe (arrows in **a**). **(c)** Follow-up axial CT image at the lateral ventricles obtained 5 years later shows asymmetric worsening atrophy (arrows) on the right. **(d)** Axial CT image shows similar asymmetric worsening at the temporal lobes. **(e, f)** Coronal **(e)** and sagittal **(f)** ^{18}F-FDG PET images obtained on the same day as the CT images show corresponding decreased activity in the frontal and temporal regions, findings compatible with FTLD. Image insets show a coronal section through the middle of the brain in this particular case to aid in lateralization.

Vascular Dementia

Although not truly a primary neurodegenerative disease, vascular-induced dementia is common and is important to consider in the differential diagnosis for patients with neurocognitive impairment. It is accepted as being the second overall most common cause of clinical dementia (53). The underlying pathophysiology is related to neural loss from impaired circulation, the most classic being multiple ischemic infarcts. The entity referred to as Binswanger disease, or subcortical arteriosclerotic encephalopathy, falls into this category.

Clinical diagnosis can be difficult, as the range of symptoms and onset vary depending on the involved regions. Development of impaired cognition with focal neurologic deficits is fairly easy to identify clinically, but if the vascular insults are small and cumulative over a long time, this can be difficult to differentiate from a primary dementing disorder. The classically taught presentation is a stepwise dementia with punctuated time intervals of progressively worsening cognition, although this is variable (54).

MR images show typical findings of vascular insults, such as encephalomalacia from multiple vascular territory infarcts, strategically placed infarcts, and white matter changes (Fig 21) (55). There are usually secondary signs of volume loss with enlargement of the ipsilateral sulci and lateral ventricle. Numerous sets of diagnostic criteria have been proposed, such as the *Diagnostic and Statistical Manual of Mental Disorders*, fourth edition (DSM-IV), and National Institute of Neurological Disorders and Stroke (NINDS)–Association Internationale pour la Recherche et l'Enseignement en Neurosciences (AIREN) criteria (56,57). ^{18}F-FDG PET shows findings of hypometabolism correlating to abnormal areas at structural imaging (Fig 22).

Other Dementing Disorders

Although the previously discussed disorders are some of the most common dementing disorders, there are many other diseases that should be considered. Normal pressure hydrocephalus is relatively common and can sometimes be confused clinically

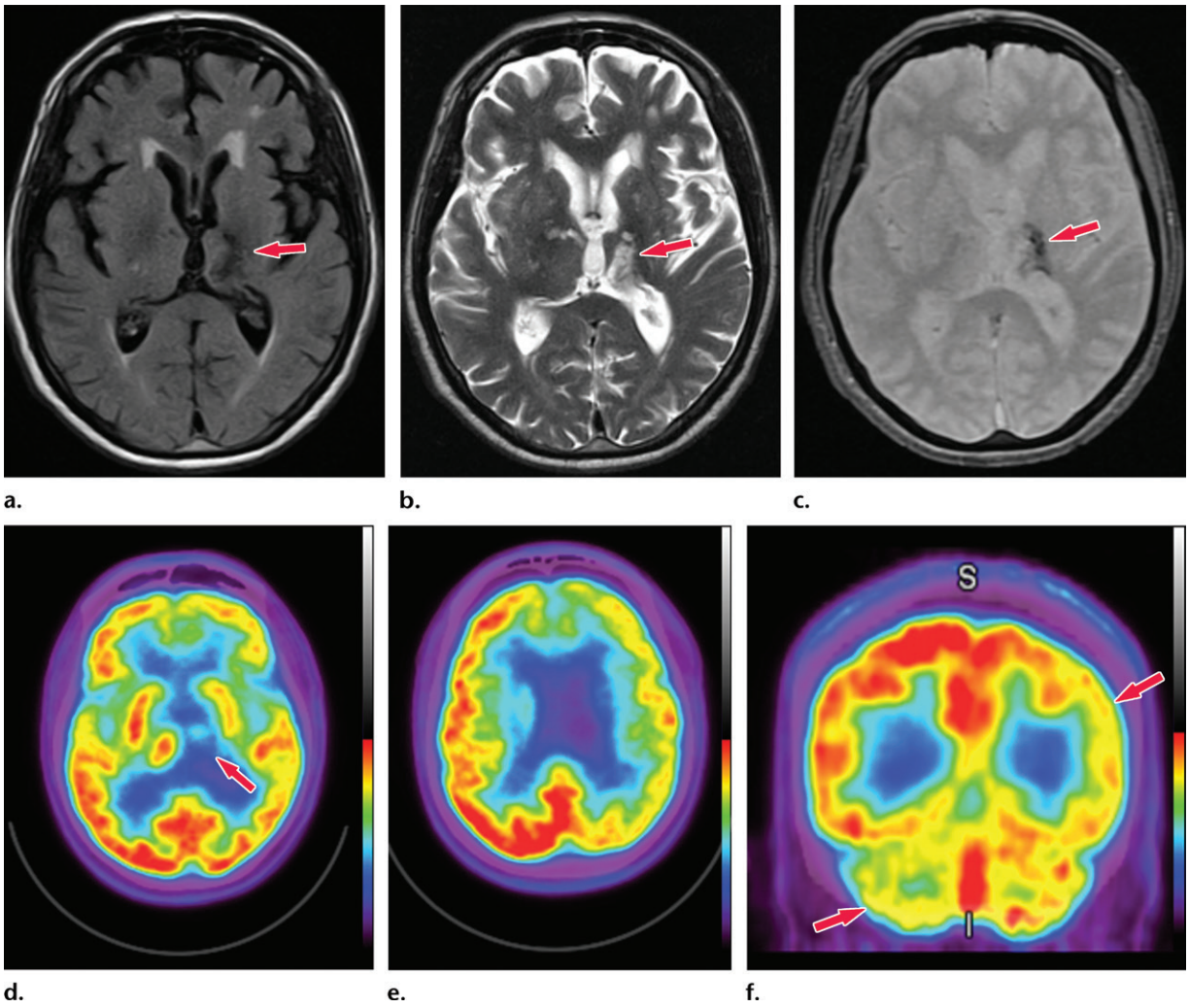

Figure 21. Patient with vascular dementia from a strategic left thalamic hemorrhagic infarct. **(a–c)** Axial T2-weighted fluid-attenuated inversion-recovery (FLAIR) **(a)**, T2-weighted **(b)**, and gradient-recalled-echo **(c)** MR images show encephalomalacia and hemosiderin staining in the left thalamus (arrow), compatible with a chronic hemorrhagic infarct. **(d, e)** Axial ^{18}F-FDG PET images at the level of the thalami **(d)** and lateral ventricles **(e)** show nearly absent activity in the left thalamus (arrow in **d**) and decreased activity in the left cerebral hemisphere, respectively, when compared with the normal activity depicted in the right thalamus and right cerebral hemisphere. Corroborative findings are compatible with thalamic infarct and vascular dementia. **(f)** Coronal ^{18}F-FDG PET image shows decreased activity (arrows) in the left cerebral hemisphere and right cerebellar hemisphere, compatible with crossed cerebellar diaschisis. This is secondary to wallerian degeneration of the white matter tracts, which decussate contralaterally. *I* = inferior, *S* = superior.

with other forms of dementia. This has characteristic imaging findings that should be identified at structural imaging to direct the patient toward appropriate management (Fig 23). In patients with rapidly progressive dementia, the diagnosis of Creutzfeldt–Jakob disease should be considered, and relatively characteristic imaging findings at structural imaging should guide the diagnosis (Fig 24). Patients with parkinsonian symptoms, the Parkinson-plus diseases, should be considered, including multiple system atrophy, corticobasal degeneration, and progressive supranuclear palsy.

Patient Workup, Algorithm, and Recommendations

In the workup for dementia and neurodegenerative processes with neuroimaging, it is important to have a good relationship with referring physicians and an algorithm for recommendations. Triaging patients to receive dedicated imaging frequently occurs with clinical assessment, although these patients can be identified by the radiologist at CT or MRI performed for other indications. For this reason, it is important that all radiologists have a working knowledge of the basic findings to allow identification of these patients, so they can receive adequate medical evaluation and treatment. Accurate workup also requires a thorough knowledge of the appearance of different processes at different imaging modalities (Table 4).

Workup can begin with either identification by the radiologist and nuclear medicine physician or direct referral from a clinician. At our

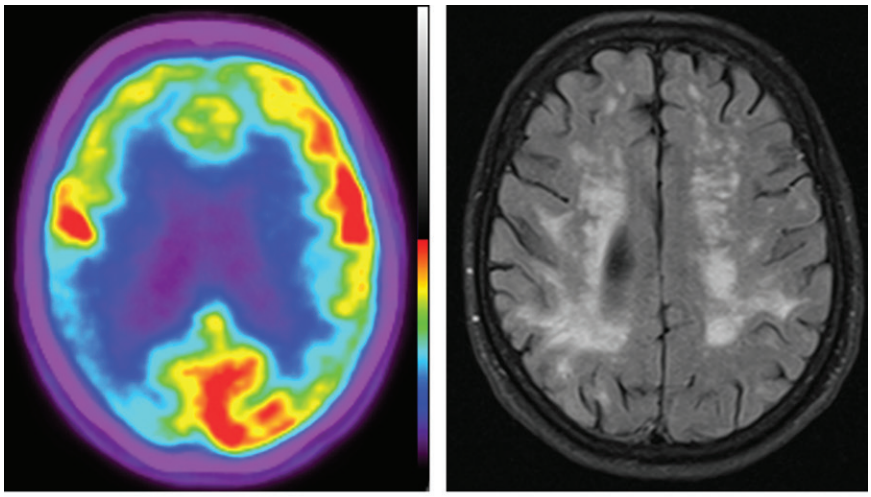

a. b.

Figure 22. Patient with vascular dementia. **(a)** Axial ^{18}F-FDG PET image shows decreased activity in the bilateral frontal and parietal regions, with the right side being worse than the left. In the proper clinical setting, these findings are suggestive of Alzheimer disease dementia. **(b)** Corresponding axial MR image shows confluent T2-weighted fluid-attenuated inversion-recovery (FLAIR) white matter areas of hyperintensity extending to the subcortical regions, reflecting extensive ischemic damage without cortical volume loss. Findings at structural and functional imaging are representative of subcortical arteriosclerotic encephalopathy or Binswanger disease.

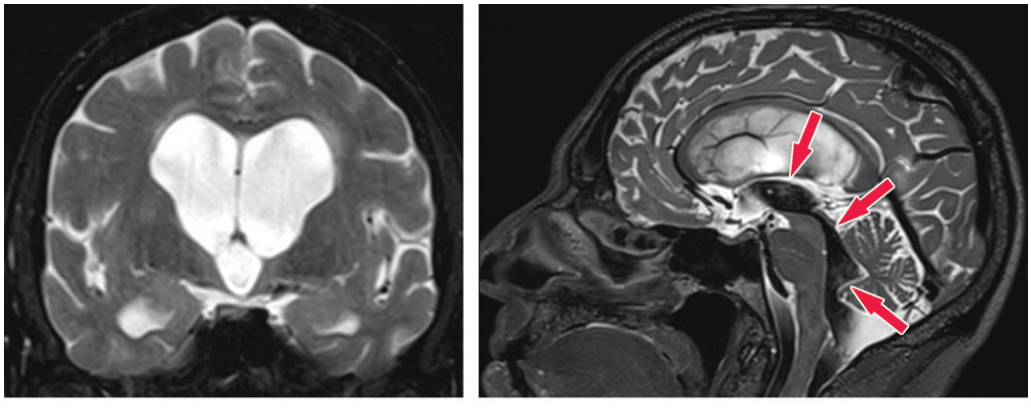

a. b.

Figure 23. Patient with normal pressure hydrocephalus with insidious onset of dementia, gait disturbance, and urinary incontinence. Coronal T2-weighted **(a)** and sagittal T2-weighted three-dimensional–volumetric high-spatial-resolution **(b)** MR images show ventriculosulcal disproportion, which is suggestive of normal pressure hydrocephalus. Three-dimensional–volumetric high-spatial-resolution images also show a large cerebrospinal fluid flow void (arrows) at the level of the third ventricle, cerebral aqueduct, and fourth ventricle, suggesting increased velocities and excluding obstruction, which helps confirm normal pressure hydrocephalus.

institution, we recommend that the first step in evaluation should be performing dedicated structural imaging for all patients with a suspected dementing neurodegenerative disorder. This allows the identification and exclusion of other processes, and in some cases may be highly supportive of a neurodegenerative diagnosis. We also typically perform FDG PET to further elucidate any region-specific abnormalities, although patients presenting with clinically apparent parkinsonian symptoms may benefit from an initial ioflupane examination. For many patients, the combination of structural imaging and FDG PET allows identification of a particular disease process. For those patients in whom the appearance is more ambiguous, β-amyloid imaging is recommended. Amyloid deposition, although not specific, can be helpful by using its negative predictive value to increase the likelihood of a non–Alzheimer disease diagnosis. Although not yet widely available, dedicated τ imaging will likely play a similar role, perhaps with greater sensitivity and specificity than those of amyloid imaging. If FDG PET imaging has findings suggestive of DLB, performing imaging with ioflupane is recommended for confirmation (Fig 25).

Table 4: Pathophysiology and Imaging Findings of Neurodegenerative Diseases

Entity	Pathophysiology	Classic Imaging Findings
Alzheimer disease	β-amyloid plaques Neurofibrillary tangles and 3R and 4R τ isoform aggregates	MRI and FDG PET: cortical loss in the temporoparietal distribution with predilection for the mesial temporal lobe and precuneus, with sparing of the sensorimotor strip Ioflupane SPECT: normal uptake Amyloid PET: abnormal amyloid tracer uptake diffusely within the cortex (loss of gray-white differentiation) τ PET: abnormal τ accumulation following the Braak staging system, with later stages similar to those abnormalities depicted at MRI and FDG PET
DLB	Abnormal α-synuclein deposition Nigrostriatal degeneration and loss of dopaminergic neurons	MRI and FDG PET: cortical loss classically beginning in the occipital lobes, with sparing of the posterior cingulate gyrus (cingulate island sign) Ioflupane SPECT: loss of uptake in the bilateral basal ganglia starting in the putamen and tracking anteriorly to the caudate head, creating a period appearance Amyloid PET: some cases demonstrate abnormal uptake τ PET: no abnormal uptake should be depicted
FTLD	Neurofibrillary tangles and abnormal τ isoform aggregates	MRI and FDG PET: cortical loss most prominent in the anterior frontal and temporal lobes, with relative sparing of the parietal lobes Ioflupane SPECT: normal uptake Amyloid PET: classically shows no abnormal uptake, although a positive examination does not exclude this diagnosis τ PET: role is currently unclear, as uptake seems to vary among different subtypes
Vascular dementia	Brain tissue infarction from trauma, toxins, or vascular insult	MRI and FDG PET: variable appearance with multifocal abnormalities asymmetrically in the regions affected Ioflupane SPECT: normal uptake Amyloid PET: no expected abnormal uptake, but a positive examination does not exclude this diagnosis τ PET: Research suggests this modality plays a role in imaging suspected chronic traumatic encephalopathy, but otherwise no uptake is expected

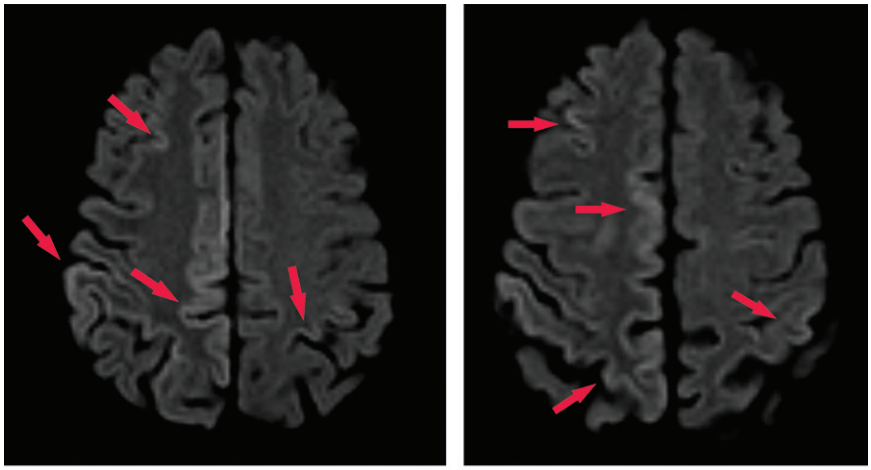

a. **b.**

Figure 24. Creutzfeldt–Jakob disease. Axial diffusion-weighted MR images in a patient with rapidly progressive dementia show gyriform areas of hyperintensity of the cortical ribbon sign (arrows), a finding suspicious for Creutzfeldt–Jakob disease. The diagnosis was confirmed on the basis of clinical and imaging findings and elevated cerebrospinal fluid 14-3-3 protein levels.

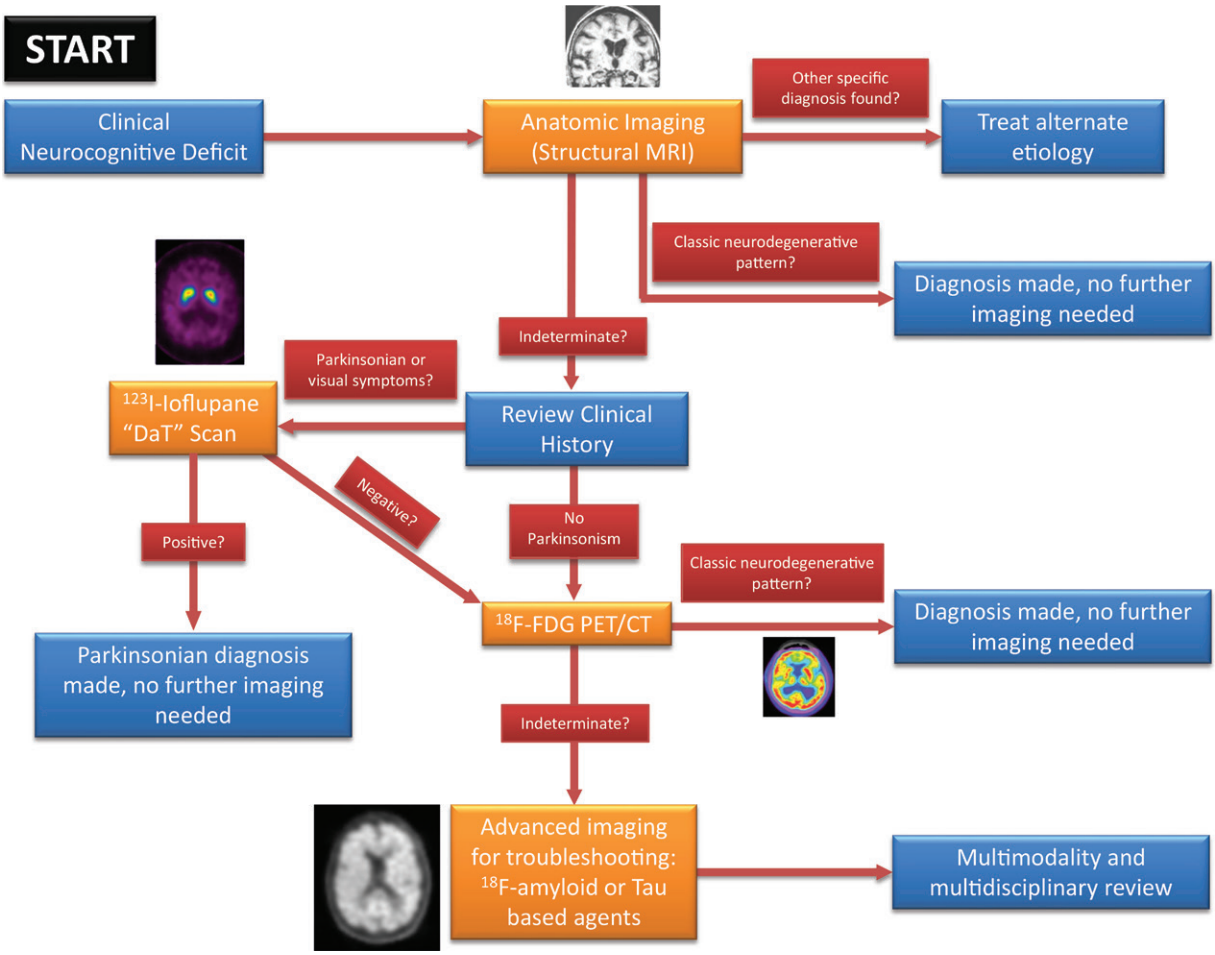

Figure 25. Flowchart shows the diagnostic strategy for the workup of patients with suspected dementia. In patients with clinical neurocognitive impairment, the first step in imaging should be performing structural MRI. This allows identification of alternate treatable causes before performing additional workup. If a diagnosis is not clear, a clinical history review should be performed to identify any parkinsonian symptoms. If these symptoms are present, a ^{123}I-ioflupane SPECT image should be obtained. If this is negative or if parkinsonian symptoms are absent, FDG PET should be performed. In many cases, the combination of MRI, FDG PET, and clinical history review findings are sufficient to suggest a diagnosis. Additional workup should be used for troubleshooting. Amyloid or τ imaging (if available) should be considered to identify patterns that would suggest an Alzheimer disease diagnosis. If the distribution on FDG images suggests DLB, an examination with ioflupane can be considered. *DaT* = dopamine transporter.

Conclusion

Dementing neurodegenerative disorders are a diverse and clinically devastating group of diseases. It is important that practicing radiologists and nuclear medicine physicians have knowledge of the findings and available imaging modalities to appropriately identify these diseases and triage these patients. Although treatment of many of these disorders is difficult with the end prognosis still being poor, there are differences in treatment and clinical expectations that are important for management. Moreover, having the ability to offer objective evidence for a particular diagnosis can be helpful both for physicians in identifying and excluding other causes and for patients and families so they can be correctly informed and prepared to avoid unnecessary hardship, both emotionally and financially. This is particularly important given the high and increasing prevalence of these diseases, and radiologists and nuclear medicine physicians are an integral component in providing valuable service to these patients and families.

Acknowledgments.—The authors will like to give special acknowledgment to Raymond James LaRue, Gainesville, Fla, for his contribution of original artwork (Figures 2, 7, and 13). The authors would like to give special acknowledgment to Jeffrey Sachs, MD, Winston-Salem, N.C., for contributing the images used in Figure 8. The authors would like to give special acknowledgment to Warren Barker, Miami Beach, Fla, and Benoit Giasson, PhD, Gainesville, Fla, for contributions of original pathology slides (Figures 11, 12) for work that was supported by the National Institute on Aging Grant, number 5 P50 AG0477266021, Florida Alzheimer's Disease Research Center (Todd Golde, PI).

References

1. Alzheimer's Association. 2019 Alzheimer's Disease Facts and Figures. Alzheimers Dement 2019;15(3):321-87.
2. Bradford A, Kunik ME, Schulz P, Williams SP, Singh H. Missed and delayed diagnosis of dementia in primary care: prevalence and contributing factors. Alzheimer Dis Assoc Disord 2009;23(4):306–314.

3. Frisoni GB, Fox NC, Jack CR Jr, Scheltens P, Thompson PM. The clinical use of structural MRI in Alzheimer disease. Nat Rev Neurol 2010;6(2):67–77.
4. Morris JC, Csernansky J, Price JL. MRI measures of entorhinal cortex versus hippocampus in preclinical AD. Neurology 2002;59(9):1474–1475; author reply 1474–1475.
5. Shen Q, Loewenstein DA, Potter E, et al. Volumetric and visual rating of magnetic resonance imaging scans in the diagnosis of amnestic mild cognitive impairment and Alzheimer's disease. Alzheimers Dement 2011;7(4):e101–e108.
6. Karas G, Scheltens P, Rombouts S, et al. Precuneus atrophy in early-onset Alzheimer's disease: a morphometric structural MRI study. Neuroradiology 2007;49(12):967–976.
7. Scheltens P, Leys D, Barkhof F, et al. Atrophy of medial temporal lobes on MRI in "probable" Alzheimer's disease and normal ageing: diagnostic value and neuropsychological correlates. J Neurol Neurosurg Psychiatry 1992;55(10):967–972.
8. Scheltens P, Launer LJ, Barkhof F, Weinstein HC, van Gool WA. Visual assessment of medial temporal lobe atrophy on magnetic resonance imaging: interobserver reliability. J Neurol 1995;242(9):557–560.
9. Urs R, Potter E, Barker W, et al. Visual rating system for assessing magnetic resonance images: a tool in the diagnosis of mild cognitive impairment and Alzheimer disease. J Comput Assist Tomogr 2009;33(1):73–78.
10. Albert M, DeCarli C, DeKosky S, et al. The Use of MRI and PET for Clinical Diagnosis of Dementia and Investigation of Cognitive Impairment: A Consensus Report—Report of the Neuroimaging Work Group of the Alzheimer's Association. Published 2005. https://www.alz.org/national/documents/imaging_consensus_report.pdf. Accessed January 9, 2019.
11. Dukart J, Mueller K, Horstmann A, et al. Combined evaluation of FDG-PET and MRI improves detection and differentiation of dementia. PLoS One 2011;6(3):e18111.
12. Waxman AD, Herholz K, Lewis MD, et al. Society of Nuclear Medicine Procedure Guideline for FDG PET Brain Imaging, Version 1.0. Society of Nuclear Medicine and Molecular Imaging. http://s3.amazonaws.com/rdcms-snmmi/files/production/public/docs/Society%20of%20Nuclear%20Medicine%20Procedure%20Guideline%20for%20FDG%20PET%20Brain%20Imaging.pdf. Approved February 8, 2009. Accessed January 26, 2019.
13. Mestre-Torres J, Lorenzo-Bosquet C, Cuberas-Borrós G, et al. Utility of the ^{18}F-Florbetapir positron emission tomography in systemic amyloidosis. Amyloid 2018;25(2):109–114.
14. Catafau AM, Bullich S. Amyloid PET imaging: applications beyond Alzheimer's disease. Clin Transl Imaging 2015;3(1):39–55.
15. Bullich S, Catafau AM, Villemagne VL, Rowe CC, Santi SD. Optimal Reference Region To Measure Longitudinal Amyloid-Beta Change With 18F-Florbetaben Pet. Alzheimers Dement 2016;12(7 suppl):P14.
16. Hsiao IT, Huang CC, Hsieh CJ, et al. Correlation of early-phase 18F-florbetapir (AV-45/Amyvid) PET images to FDG images: preliminary studies. Eur J Nucl Med Mol Imaging 2012;39(4):613–620.
17. Minoshima S, Drzezga AE, Djekidel M, et al. SNMMI Procedure Standard-EANM Practice Guideline for Amyloid PET Imaging of the Brain. Society of Nuclear Medicine and Molecular Imaging. http://s3.amazonaws.com/rdcms-snmmi/files/production/public/ACNM/Documents/SNMMI-EANM%20Standard%20for%20Amyloid%20PET%20Imaging%20of%20the%20Brain%20_1535555859659_26.pdf. Approved January 30, 2016. Accessed January 26, 2019.
18. Djang DSW, Janssen MJR, Bohnen N, et al. SNM Practice Guideline for Dopamine Transporter Imaging with 123I-Ioflupane SPECT 1.0*. Society of Nuclear Medicine and Molecular Imaging. http://s3.amazonaws.com/rdcms-snmmi/files/production/public/docs/123I_ioflupane_SPECT_Practice_Guideline_JNM_Edit_FINAL.pdf. Approved October 26, 2011. Accessed January 26, 2019.
19. Leuzy A, Chiotis K, Lemoine L, et al. Tau PET imaging in neurodegenerative tauopathies—still a challenge. Mol Psychiatry 2019;24(8):1112–1134.
20. Lowe VJ, Curran G, Fang P, et al. An autoradiographic evaluation of AV-1451 Tau PET in dementia. Acta Neuropathol Commun 2016;4(1):58.
21. Dickstein DL, Pullman MY, Fernandez C, et al. Cerebral [^{18} F]T807/AV1451 retention pattern in clinically probable CTE resembles pathognomonic distribution of CTE tauopathy. Transl Psychiatry 2016;6(9):e900.
22. Kakimoto A, Kamekawa Y, Ito S, et al. New computer-aided diagnosis of dementia using positron emission tomography: brain regional sensitivity-mapping method. PLoS One 2011;6(9):e25033.
23. Mckee AC, Abdolmohammadi B, Stein TD. The neuropathology of chronic traumatic encephalopathy. Handb Clin Neurol 2018;158:297–307.
24. Irwin DJ. Tauopathies as clinicopathological entities. Parkinsonism Relat Disord 2016;22(Suppl 1):S29–S33.
25. Wang S, Mims PN, Roman RJ, Fan F. Is Beta-Amyloid Accumulation a Cause or Consequence of Alzheimer's Disease? J Alzheimers Parkinsonism Dement 2016;1(2):007.
26. Shimada H, Shinotoh H, Hirano S, et al. β-Amyloid in Lewy body disease is related to Alzheimer's disease-like atrophy. Mov Disord 2013;28(2):169–175.
27. Gomperts SN, Rentz DM, Moran E, et al. Imaging amyloid deposition in Lewy body diseases. Neurology 2008;71(12):903–910.
28. Tan RH, Kril JJ, Yang Y, et al. Assessment of amyloid β in pathologically confirmed frontotemporal dementia syndromes. Alzheimers Dement (Amst) 2017;9:10–20.
29. Yan F, Chen Y, Li M, et al. Gastrointestinal nervous system α-synuclein as a potential biomarker of Parkinson disease. Medicine (Baltimore) 2018;97(28):e11337.
30. Qiu C, Kivipelto M, von Strauss E. Epidemiology of Alzheimer's disease: occurrence, determinants, and strategies toward intervention. Dialogues Clin Neurosci 2009;11(2):111–128.
31. Leon J, Cheng CK, Neumann PJ. Alzheimer's disease care: costs and potential savings. Health Aff (Millwood) 1998;17(6):206–216.
32. Jia J, Wei C, Chen S, et al. The cost of Alzheimer's disease in China and re-estimation of costs worldwide. Alzheimers Dement 2018;14(4):483–491.
33. Murphy MP, LeVine H 3rd. Alzheimer's disease and the amyloid-β peptide. J Alzheimers Dis 2010;19(1):311–323.
34. Braak H, Alafuzoff I, Arzberger T, Kretzschmar H, Del Tredici K. Staging of Alzheimer disease-associated neurofibrillary pathology using paraffin sections and immunocytochemistry. Acta Neuropathol (Berl) 2006;112(4):389–404.
35. McKhann GM, Knopman DS, Chertkow H, et al. The diagnosis of dementia due to Alzheimer's disease: recommendations from the National Institute on Aging-Alzheimer's Association workgroups on diagnostic guidelines for Alzheimer's disease. Alzheimers Dement 2011;7(3):263–269.
36. Braak H, Braak E. Neuropathological stageing of Alzheimer-related changes. Acta Neuropathol (Berl) 1991;82(4):239–259.
37. Laforce R Jr, Soucy JP, Sellami L, et al. Molecular imaging in dementia: Past, present, and future. Alzheimers Dement 2018;14(11):1522–1552.
38. Rabinovici GD, Furst AJ, Alkalay A, et al. Increased metabolic vulnerability in early-onset Alzheimer's disease is not related to amyloid burden. Brain 2010;133(Pt 2):512–528.
39. Schwarz AJ, Yu P, Miller BB, et al. Regional profiles of the candidate tau PET ligand 18F-AV-1451 recapitulate key features of Braak histopathological stages. Brain 2016;139(Pt 5):1539–1550.
40. Yang SK, Chen W, Su CH, Liu CH. Incidence and Comorbidity of Dementia with Lewy Bodies: A Population-Based Cohort Study. Behav Neurol 2018;2018:7631951.
41. Donaghy PC, McKeith IG. The clinical characteristics of dementia with Lewy bodies and a consideration of prodromal diagnosis. Alzheimers Res Ther 2014;6(4):46.
42. Mak E, Su L, Williams GB, O'Brien JT. Neuroimaging characteristics of dementia with Lewy bodies. Alzheimers Res Ther 2014;6(2):18.
43. Shams S, Fällmar D, Schwarz S, et al. MRI of the Swallow Tail Sign: A Useful Marker in the Diagnosis of Lewy Body Dementia? AJNR Am J Neuroradiol 2017;38(9):1737–1741.

44. Graff-Radford J, Murray M, Lowe V, Boeve B, Ferman T. Dementia with Lewy bodies: basis of cingulate island sign. Neurology 2014;83(9):801–809.
45. Le Ber I, Guedj E, Gabelle A, et al. Demographic, neurological and behavioural characteristics and brain perfusion SPECT in frontal variant of frontotemporal dementia. Brain 2006;129(Pt 11):3051–3065.
46. Wada-Isoe K, Ito S, Adachi T, et al. Epidemiological survey of frontotemporal lobar degeneration in tottori prefecture, Japan. Dement Geriatr Cogn Disord Extra 2012;2(1):381–386.
47. Bott NT, Radke A, Stephens ML, Kramer JH. Frontotemporal dementia: diagnosis, deficits and management. Neurodegener Dis Manag 2014;4(6):439–454.
48. Cairns NJ, Bigio EH, Mackenzie IRA, et al. Neuropathologic diagnostic and nosologic criteria for frontotemporal lobar degeneration: consensus of the Consortium for Frontotemporal Lobar Degeneration. Acta Neuropathol (Berl) 2007;114(1):5–22.
49. Gordon E, Rohrer JD, Fox NC. Advances in neuroimaging in frontotemporal dementia. J Neurochem 2016;138(Suppl 1):193–210.
50. Schroeter ML, Raczka K, Neumann J, Yves von Cramon D. Towards a nosology for frontotemporal lobar degenerations-a meta-analysis involving 267 subjects. Neuroimage 2007;36(3):497–510.
51. Rohrer JD, Warren JD, Modat M, et al. Patterns of cortical thinning in the language variants of frontotemporal lobar degeneration. Neurology 2009;72(18):1562–1569.
52. Rabinovici GD, Furst AJ, O'Neil JP, et al. 11C-PIB PET imaging in Alzheimer disease and frontotemporal lobar degeneration. Neurology 2007;68(15):1205–1212.
53. Rizzi L, Rosset I, Roriz-Cruz M. Global epidemiology of dementia: Alzheimer's and vascular types. BioMed Res Int 2014;2014:908915.
54. Strub RL. Vascular dementia. Ochsner J 2003;5(1):40–43.
55. van Straaten EC, Scheltens P, Barkhof F. MRI and CT in the diagnosis of vascular dementia. J Neurol Sci 2004;226(1-2):9–12.
56. Román GC, Tatemichi TK, Erkinjuntti T, et al. Vascular dementia: diagnostic criteria for research studies. Report of the NINDS-AIREN International Workshop. Neurology 1993;43(2):250–260.
57. Sachdev P, Kalaria R, O'Brien J, et al. Diagnostic criteria for vascular cognitive disorders: a VASCOG statement. Alzheimer Dis Assoc Disord 2014;28(3):206–218.